https://doi.org/10.5194/bg-2022-207
Preprint. Discussion started: 28 October 2022

Biogeosciences Discussions

Mapping soil organic carbon fractions for Australia, their stocks and uncertainty

Mercedes Román Dobarco[1], Alexandre M.J-C. Wadoux[1], Brendan Malone[2], Budiman Minasny[1], Alex B. McBratney[1], Ross Searle[3]

[1]Sydney Institute of Agriculture & School of Life and Environmental Sciences, The University of Sydney, 1 Central Avenue, Eveleigh, 2015, NSW, Australia

[2]CSIRO Agriculture and Food, Black Mountain, ACT, Australia

[3]CSIRO Agriculture and Food, 306 Carmody Road, St Lucia, QLD, Australia.

Correspondance to: Mercedes Román Dobarco (mercedes.romandobarco@sydney.edu.au)

Abstract. Soil organic carbon (SOC) is the largest terrestrial carbon pool. SOC is composed of a continuum set of compounds with different chemical composition, origin and susceptibilities to decomposition, that are commonly separated into pools characterised by different responses to anthropogenic and environmental disturbance. Here we map the contribution of three SOC fractions to the total SOC content of Australia's soils. The three SOC fractions: mineral-associated organic carbon (MAOC), particulate organic carbon (POC) and pyrogenic organic carbon (PyOC), represent SOC composition with distinct turnover rates, chemistry, and pathway formation. Data for MAOC, POC, and PyOC were obtained with near- and mid-infrared spectral models calibrated with measured SOC fractions. We transformed the data using an isometric log-ratio transformation (ilr) to account for the closed compositional nature of SOC fractions. The resulting, back-transformed ilr components were mapped across Australia. SOC fraction stocks for the 0-30 cm were derived with maps of total organic carbon concentration, bulk density, coarse fragments and soil thickness. Mapping was done by quantile regression forest fitted with the ilr transformed data and a large set of environmental variables as predictors. The resulting maps along with the quantified uncertainty show the unique spatial pattern of SOC fractions in Australia. MAOC dominated the total SOC with an average of 59% ±17.5%, whereas 28% ± 17.5% was PyOC and 13% ± 11.1% was POC. The allocation of TOC into the MAOC fractions increased with depth. SOC vulnerability (i.e., POC/[MAOC + PyOC]) was greater in areas with Mediterranean and temperate climate. TOC and the distribution among fractions were the most influential variables on SOC fraction uncertainty. Further, the diversity of climatic and pedological conditions suggests that different mechanisms will control SOC stabilisation and dynamics across the continent, as shown by the model covariates importance metric. We estimated the total SOC stocks (0-30 cm) to be 12.7 Pg MAOC, 2 Pg POC and 5.1 Pg PyOC, which is consistent with previous estimates. The maps of SOC fractions and their stocks can be used for modelling SOC dynamics and forecasting changes in SOC stocks as response to land use change, management, and climate change.

https://doi.org/10.5194/bg-2022-207
Preprint. Discussion started: 28 October 2022

Keywords: Soil organic carbon, SOC fractions, particulate organic carbon, mineral-associated organic carbon, pyrogenic organic carbon, digital soil mapping.

1 Introduction

Soils are the main organic carbon pool in terrestrial ecosystems, storing around two thirds of the total C. Global soil organic carbon (SOC) stock is estimated to be around 1500 PgC for the first metre of soil (Jobbagy and Jackson, 2000), with other estimates ranging from 504 to 3000 PgC (Scharlemann et al., 2014). Changes in SOC storage and dynamics can alter the ecosystem C balance and determine whether soils become C sources or sinks from local to global scale (Friedlingstein et al., 2020). SOC is strongly linked to most soil properties and functions (e.g., nutrient and water storage and cycling, habitat provisioning and biodiversity) (Van Leeuwen et al., 2019), and hence is used as a general indicator of soil quality/capacity (Schoenholtz et al., 2000; Bunemann et al., 2018) and soil health/condition.

SOC is the main component of soil organic matter, which is a continuum of compounds with different chemical compositions, origin (aboveground litter, dead roots, rhizodeposition, microbial-derived), degree of microbial processing and decomposition, and turnover times (Lehmann and Kleber, 2015). SOC is protected against microbial decomposition by several stabilisation mechanisms which have been generally grouped into: 1) selective preservation due to biochemical recalcitrance, 2) chemical stabilisation via interactions between organic compounds and mineral surfaces or metal cations, and 3) physical protection by the inaccessibility of decomposers to the organic matter (Sollins et al., 1996; Von Lutzow et al., 2006; Rowley et al., 2018). Spatial inaccessibility and interactions between the mineral surfaces of silt and clay-sized particles and organic compounds are considered the major mechanisms for mid and long-term SOC stability (Von Lutzow et al., 2006), whereas an increasing body of literature questions the relevance of biochemical recalcitrance for long-term persistence of SOC (Schmidt et al., 2011). A myriad of physical, chemical, or combined fractionation methods have been designed for separating SOC into operational pools characterized by specific stabilization mechanisms, chemical composition, and distinct turnover rates, and yet it is difficult to isolate fractions that correspond to functional SOC pools (Lutzow et al., 2007). Some fractionation schemes were adapted to quantify conceptual SOC pools from established C dynamics models, e.g., the Rothamsted C model (RothC, Jenkinson and Rayner (1977)) from measured SOC fractions (Poeplau et al., 2013; Zimmermann et al., 2007). However, there can be some discrepancies between the predicted SOC pools when the model is initialized with modelled SOC pools from equilibrium runs or from measured SOC fractions (Poeplau et al., 2013). Other biogeochemical models have been conceptualized and calibrated with functional and measurable SOC fractions to overcome these differences (Robertson et al., 2019), but often require the determination of many SOC fractions. A comparison of several fractionation schemes (Poeplau et al., 2018) suggests that size separation into silt + clay (<53 µm) (i.e., mineral-associated organic carbon (MAOC)), and sand-sized particles (>53 µm) (i.e., particulate organic carbon (POC)), may suffice to differentiate pools with distinct turnover rates, chemistry, and pathway formation (Lavallee et al., 2020). MAOC is predominantly composed of low molecular weight molecules of microbial origin (e.g., microbial metabolites, necromass) (Miltner et al., 2012; Kallenbach et al., 2016; Liang et

https://doi.org/10.5194/bg-2022-207
Preprint. Discussion started: 28 October 2022

al., 2019), leachates from plant litter, and rhizodeposition (Villarino et al., 2021), which are protected through sorption to mineral surfaces or occluded inside microaggregates (Lavallee et al., 2020). POC is mainly composed of partially decomposed plant litter and roots and fungal-derived compounds (Baisden et al., 2002; Gregorich et al., 2006; Geng et al., 2019; Villarino et al., 2021), that can be found free or inside macroaggregates (Rabbi et al., 2014). MAOC has a lower C:N ratio, a higher proportion of microbial-derived and proteinaceous compounds (Kleber et al., 2007; Knicker, 2011) and a longer mean residence time (decades to centuries) than POC (mean residence time of years to decades) (Baisden et al., 2002; Gregorich et al., 2006; Von Lützow et al., 2007; Heckman et al., 2022). Separating SOC into POC and MAOC has been proposed as a simple and effective way to conceptualize and model SOC dynamics (Lavallee et al., 2020), and has been applied to predict the vulnerability of SOC to future climate scenarios (Lugato et al., 2022).

In Australia, the long history of burning suggests pyrogenic organic carbon (PyOC) as an important component (Lehmann et al., 2008). PyOC refers to charred residues derived from incomplete combustion of organic matter (also known as charcoal or black carbon) (Lutfalla et al., 2017). PyOC can be found in both POC and MAOC fractions (Lavallee et al., 2019). PyOC is comprised by a continuum of organic compounds thermically altered by fire, and its chemical composition and pool size depends on the technique used for its determination(Zimmerman and Mitra, 2017). PyOC is considered a relatively stable SOC fraction with a turnover time that ranges from decades to centuries (Singh et al., 2012), protected from decomposition by the biochemical recalcitrance of condensed aromatic C (Lavallee et al., 2019). However, turnover rates previously assessed from centuries to multi-millenia may have overestimated its persistence in soil (Singh et al., 2012; Lutfalla et al., 2017). PyOC represents on average 14-26% of total SOC and can reach up to 60-80% of SOC (Lehmann et al., 2008; Reisser et al., 2016). Globally, PyOC stocks are not controlled by fire intensity and return interval, but are explained by soil properties and climate (Reisser et al., 2016). However, in systems with local records of fire history PyOC content increased in sites with high-frequency fires (Reisser et al., 2016). In Australia, fire is an important driver of ecological processes, and bush-fire frequency has increased in recent decades (Dutta et al., 2016). Hence, PyOC can represent a large proportion of total SOC in some Australian regions (Lehmann et al., 2008).

Mapping and quantifying the stocks of SOC fractions can be used for modelling SOC dynamics and forecasting changes in SOC stocks as a response to land-use change, management, and climate change (Lugato et al., 2022; Xu et al., 2011; Wiesmeier et al., 2016). High-resolution maps of SOC fractions can inform agricultural management at the farm scale and be incorporated in the design of climate change and soil security policies at the state and national level. The objective of this study was to map the contribution of SOC fractions (MAOC, POC, and PyOC) to the total SOC in the top 30 cm and update the Soil and Landscape Grid of Australia (SLGA) (Grundy et al., 2015) products for SOC fraction stocks (Viscarra Rossel et al., 2019). These digital soil maps will be part of the v2.SLGA for Australia, following the principles of transparency, reproducibility, and updatability as new data become available (Malone and Searle, 2021).

https://doi.org/10.5194/bg-2022-207
Preprint. Discussion started: 28 October 2022

2 Materials and Methods

The methodology implemented in this study consists of two main steps: 1) prediction of SOC fractions across the soil spectral libraries available for Australia with different spectral models calibrated with measured SOC fraction data from the Australian Soil Carbon Research Program (SCaRP) (Baldock et al., 2013a), and 2) mapping of the proportions of SOC fractions after applying the isometric log-ratio transformation (ilr) to account for the compositional nature of the data (i.e., the proportion of SOC fractions sum to 100%). Previous studies modelled SOC fractions stocks or concentrations (Sanderman et al., 2021; Viscarra Rossel et al., 2019), but we found some difficulties in implementing such an approach (see Sect. 2.5) and hence mapped proportions of SOC. Finally, we calculated SOC fraction stocks for the 0-30 cm using data from SLGA maps of total organic carbon (TOC) concentration (Wadoux et al., 2022), bulk density (Viscarra Rossel et al., 2015), coarse fragments (this study) and soil thickness (Malone and Searle, 2020).

2.1 Study area

The study area covers the continent of Australia, including Tasmania and near-shore small islands. In Australia there are six major climatic regions following the Köppen classification. In the north, there are hot humid summers in equatorial, tropical and subtropical regions. Summers are hot and dry, with mild to cold winters in grasslands and desert regions in the interior. Temperate areas in the south coastal band have cold winters and warm summers, that are mild at higher elevations and latitudes. Vast areas of the continent are very dry, with precipitation increasing towards the coast and elevation in the mountains of the eastern uplands. Australia is characterised by flat and low relief vast areas where the tectonic stability and lack of glaciation have preserved a deeply weathered mantle that dates from the Tertiary (Mckenzie et al., 2004). The distribution of soils in many regions depends on the stripping of this weathered mantle, while in other areas the dominant drivers of landforms and soils are water, fluvial, and aeolian erosion and depositional processes (McKenzie et al., 2004). Younger soils are found mainly in the east, along the Great Divide (McKenzie et al., 2004). The dominant soil orders according to the Australian Soil Classification (Isbell et al., 1997) are Kandosol (30 % of the area), Tenosol (20 %), Vertosol (14 %), Rudosol (8 %), Calcarosol (8 %) and Chromosol (7 %) (Searle, 2021). In 2015-2016 most of the area was dedicated to primary production, with 48 % of the continent used for livestock grazing (42 % on native vegetation and 6 % modified pastures), less than 5 % dedicated to dryland and irrigated cropping. About 9.5% of Australia is allocated to nature conservation and 18 % are protected managed resources (ABARES, 2022).

2.2 SCaRP dataset – sampling design and SOC fractionation scheme

The soil sampling design and SOC fractionation protocol of SCaRP are described in detail in Sanderman et al. (2011) and Baldock et al. (2013c). The objective of SCaRP was to characterize SOC stocks and composition of agricultural topsoils (0-30 cm) and their response to agricultural practices. Plots of 25 m^2 were laid in 4526 sites representative of the different combinations of agricultural management and soil types across Australia. At each plot, soil samples were collected randomly

https://doi.org/10.5194/bg-2022-207
Preprint. Discussion started: 28 October 2022

at 10 nodes of a 5 m x 5 m grid with a soil corer (≥ 4 cm diameter) by depth interval (0-10, 10-20, 20-30 cm) and composited by layer. In addition, at least three measurements of bulk density by depth interval were taken at each plot, although the methods varied between states to accommodate the soil type. A subset of 312 samples representative of the range of TOC content found among the whole dataset (N = 24,495 samples) were subject to fractionation (Baldock et al., 2013c). The size and chemical fractionation scheme divided SOC into MAOC, POC and PyOC. MAOC and PyOC were originally defined as humic organic carbon and resistant organic carbon in Baldock et al. (2013c) but we changed the terminology to match the recent literature. A 10-g aliquot of air-dried soil ≤ 2 mm was dispersed with 5 g L^{-1} sodium hexametaphosphate and separated into coarse (>50 µm) and fine (<50 µm) fractions with wet sieving using an automated sieve shaker system (Baldock et al., 2013b). The TOC concentrations of the coarse and fine fractions were analysed with high-temperature oxidative combustion after the removal of inorganic carbon with 5-6 % H_2SO_3 if carbonates were present (method 6B3a, Rayment and Lyons (2011)). The content of poli-aryl C was determined with solid-state ^{13}C NMR (nuclear magnetic resonance spectroscopy) and used as an estimate of PyOC. POC and MAOC contents (mg C-fraction g^{-1} soil) were calculated by subtracting the proportion of PyOC in each fraction (Baldock et al., 2013c).

2.3 Spectral datasets and harmonization

Four spectral soil datasets were combined in this study: SCaRP, the Australian Soil Archive mid-infrared (MIR) spectral library (AusSpecMIR) (Hicks et al., 2015), an additional MIR library of specimens from the Australian Soil Archive that were not included in the Hicks et al. (2015) work (AusSpecMIR2) and the Australian Soil Archive visible and near-infrared (vis-NIR) spectral library (AusSpecNIR) (Viscarra Rossel and Hicks, 2015).

Multiple soil samples (approximately 700) were represented both in AusSpecMIR and AusSpecNIR, and duplicates were removed from the AusSpecNIR for the subsequent modelling. The AusSpecNIR library includes 433 samples from SCaRP. The soil samples come from different soil surveys and projects carried out by Australian states and federal agencies. Notably, the AusSpecNIR includes samples from the Terrestrial Ecosystem Research Network (TERN) Ecosystem Surveillance plots (Sparrow et al., 2020; Malone et al., 2020), increasing the representation of non-agricultural soils (rangelands, forests) in the calibration data (Figure 1). Vegetation and soils are sampled in more than 800 permanent plots laid with stratified random sampling across bioregions (i.e., zones with similar landform, vegetation, and climate, analogous to ecoregion) (Sparrow et al., 2020). Soil samples are taken from three depth intervals (0-10, 10-20, 20-30 cm) in nine locations within a 100 m x 100 m plot (Sparrow et al., 2020), for a total of 15,157 soil samples at 5,711 georeferenced sampling points.

https://doi.org/10.5194/bg-2022-207
Preprint. Discussion started: 28 October 2022

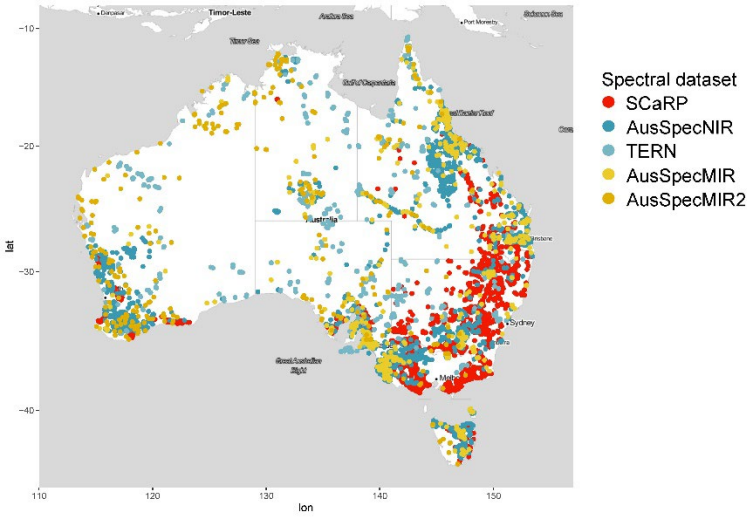

Figure 1: Soil spectral datasets combined for mapping soil organic carbon fractions. TERN samples are part of the AusSpecNIR library.

The SCaRP spectral library was produced with a Nicolet 6700 FTIR spectrometer (Thermo Fisher Scientific Inc., Waltham, MA, USA) equipped with a KBr beam-splitter, a DTGS detector and an AutoDiff Automated diffuse reflectance accessory (Pike Technologies, Madison, WI, USA). Spectra were acquired over the range 8000-400 cm^{-1} with a resolution of 8 cm^{-1}. The spectrum of each soil sample was the average of 60 scans. The AusSpecMIR spectral library was created with a Bruker FT-IR Vertex70 spectrometer. This instrument is fitted with a mercury cadmium telluride detector that is liquid N_2 cooled to improve signal-to-noise ratio and has a spectral range of 7500-600 cm^{-1} at 4 cm^{-1} resolution. AusSpecMIR2 were measured with a Bruker FT-IR Invenio spectrometer with a similar liquid N_2 cooling system and spectral range of 7500-600 cm^{-1} at 4 cm^{-1} resolution. Soil samples from AusSpecMIR and AusSpecMIR2 were scanned per quadruplicate. Diffuse reflectance spectra for the AusSpecNIR library were collected with a Labspec® vis–NIR spectrometer (PANalytical Inc., Boulder, CO, USA) for the range 350–2500 nm at 1 nm resolution. Each spectrum was the average of 30 scans and 4 spectra were collected for each soil sample (Viscarra Rossel and Hicks, 2015). To apply the SOC fraction predictive models calibrated with SCaRP data to the spectral datasets measured with a different instrument, we harmonised the spectra from SCaRP, AusSpecMIR and AusSpecMIR2 with piecewise direct standardization (PDS) (Bouveresse and Massart, 1996; Ge et al., 2011). Approximately 200 soil samples from the SCaRP dataset were measured with the Bruker FT-IR Vertex70 spectrometer, following the estimate of parameters to harmonise the SCaRP library with AusSpecMIR. Similarly, the AusSpecMIR2 was harmonised with AusSpecMIR with PDS using a standard of 300 soil samples measured with both instruments (Table 1).

https://doi.org/10.5194/bg-2022-207
Preprint. Discussion started: 28 October 2022

2.4 Spectral models and predictions of SOC fractions

SOC fractions contents (mg C g^{-1} soil) of SCaRP samples were estimated with partial least squares regression (PLSR) models developed by Baldock et al. (2013b). Baldock et al. (2013b) reported cross-validation results (squared-root transformed SOC fraction contents) with R^2 values of 0.84, 0.88 and 0.85, and RMSE of 0.43, 0.40 and 0.32 for POC, MAOC and PyOC respectively.

SOC fractions content for AusSpecMIR and AusSpecMIR2 were estimated with a new set of spectral predictive functions. These functions were developed with 200 SCaRP samples with data on SOC fractions concentration (mg C-SOC fraction g^{-1} soil), total organic carbon (TOC) concentration (mg C g^{-1} soil), and harmonised spectra. The contents of SOC fractions were converted into percentages of TOC (summing up to 100 %) and modelled as compositional data. Hence, the ilr transformation was applied to the proportions of SOC fractions. The ilr generates a D-1 dimensional Euclidean vector, where D is the number of variables in the original variables (Aitchison, 1986). PLSR models with bootstrapping were used to predict the ilr-transformed SOC fractions. Validation statistics were calculated from the average of 50 model realisations on the back-transformed data. The average RMSE for POC, MAOC and PyOC were 6.2, 7.7, and 6.4 %, respectively. The Lin's concordance correlation coefficient (ρ_c) values were 0.86, 0.76 and 0.70, and R^2 of 0.74, 0.61, and 0.52. When the percentages were back-transformed into SOC fraction contents (mg C-SOC fraction g^{-1} soil), the RMSE were 2.1, 2.7, and 1.8 mg C g^{-1} soil, ρ_c of 0.92, 0.95, and 0.90, and R^2 of 0.85, 0.88, and 0.77 for POC, MAOC and PyOC respectively.

SOC fraction contents for the AusSpecNIR dataset were predicted with PLSR models calibrated with data on TOC concentration and SOC fractions contents from 309 SCaRP samples. Before modelling, the spectra were trimmed to the 453-2500 nm range, processed with a Savitsky-Golay smoothing filter and transformed from reflectance to absorbance. We also applied the standard normal variate transformation and then wavelet coefficients were derived. Similarly, as for the MIR datasets, spectral predictive functions were developed for ilr-transformed SOC fraction compositional data, and validation statistics were calculated for the back-transformed data. The validation statistics for POC, MAOC and PyOC models were respectively RMSE of 5.0, 6.4, and 5.8 %, ρ_c of 0.92, 0.84, and 0.76, and R^2 of 0.83, 0.71, and 0.61 when validated as proportions of TOC. When the validation statistics were calculated for SOC fraction contents, the RMSE were 3.2, 4.0 and 2.3 mg C g^{-1} soil and ρ_c of 0.81, 0.87, 0.80, and R^2 of 0.65, 0.75 and 0.64 for POC, MAOC and PyOC.

Table 1: Spectral datasets, harmonization and spectral predictive models used to map soil organic carbon fractions.

Dataset	Number of Sites	Number of soil samples	Spectra	Spectra harmonization	Spectral model	Reference
SCaRP	4498	14426	MIR	From SCaRP to AusSpecMIR with 200	PLSR developed with 312 samples	Baldock et al. (2013b)

https://doi.org/10.5194/bg-2022-207
Preprint. Discussion started: 28 October 2022

				samples scanned with both spectrometers		
AusSpecMIR	3976	719	MIR	Standard	PLSR developed with 200 samples from SCaRP dataset. Models for ilr-transformed variables.	Malone and Wadoux (2021)
AusSpecMIR2	337	300	MIR	From AusSpecMIR2 to AusSpecMIR with 300 samples scanned with both spectrometers		
AusSpecNIR	9,289	22,684	Vis-NIR		PLSR developed with 309 samples from SCaRP dataset. Models for ilr-transformed variables.	Malone (2021)

200

2.5 SOC fractions data processing and depth standardisation

The georeferenced SOC fraction data from all libraries was projected to WGS 84 (EPSG:4326) and collated. The data were filtered and processed to harmonize units, duplicates and potentially wrong data entries (e.g., missing upper or lower horizon depths) were excluded. SOC predictions of the quadruplicated scans per soil sample were averaged, as well as multiple soil
205 samples per horizon by sampling location. SOC fraction concentrations (mg C-SOC fraction g^{-1} soil) were transformed to proportion of total SOC (% SOC). SOC vulnerability (Vp) was defined as the ratio of POC to the sum of MAOC and PyOC (Baldock et al., 2018), i.e., the proportion of the less protected SOC fraction (POC) to the SOC fractions with stability by physico-chemical protection and recalcitrance, and longer turnover rates. SOC fractions and Vp data were standardized to the first three depth intervals of the GlobalSoilMap specifications (0-5 cm, 5-15 cm, 15-30 cm) (Arrouays et al., 2014) with equal-
210 area quadratic splines (Bishop et al., 1999) (Figure 2). For sampling locations with just one sampled horizon, this was converted to the GlobalSoilMap depth intervals (assigned to a single or several depth intervals) via aggregation with the *slab* function of the *aqp* R package (Beaudette et al., 2022). We calculated the mean and standard deviation of SOC fractions and Vp by GlobalSoilMap depth interval and by biome (Olson et al., 2001).

https://doi.org/10.5194/bg-2022-207
Preprint. Discussion started: 28 October 2022

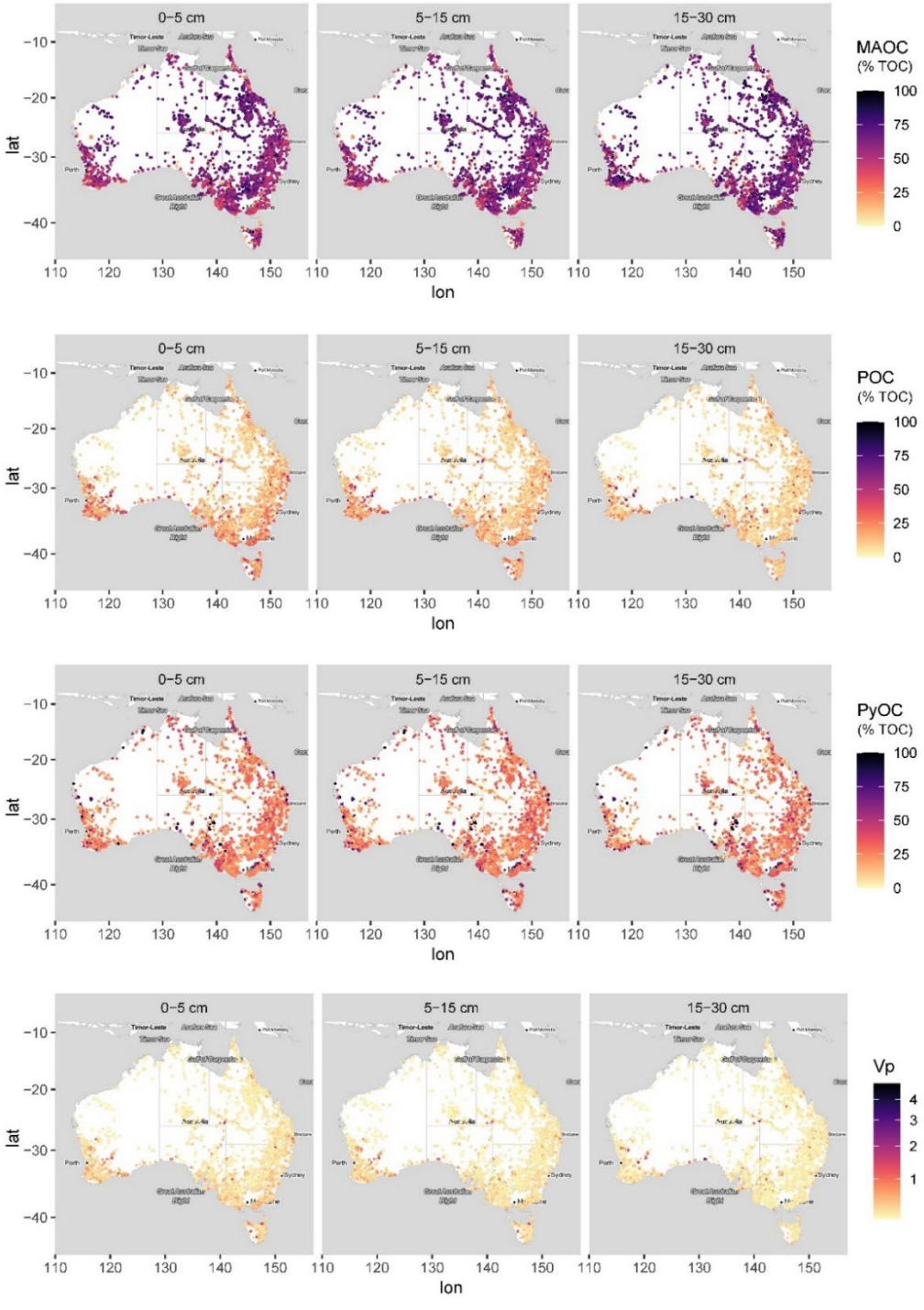

Figure 2: Calibration data standardized for the depths 0-5 cm, 5-15 cm, and 15-30 cm. Contribution of SOC fractions to total organic carbon (% TOC): mineral-associated SOC (MAOC), particulate organic carbon (POC), pyrogenic organic carbon (PyOC) and soil organic carbon vulnerability (Vp).

https://doi.org/10.5194/bg-2022-207
Preprint. Discussion started: 28 October 2022

Modelling SOC fraction concentrations directly was the preferred option tested in preliminary work. We compared the sum of the predicted SOC fraction contents with measured TOC. The Pearson's *r* correlation coefficient was 0.56, but the sum of SOC fractions showed some extreme values (Figure S1). We adjusted the SOC fraction contents with measured TOC data extracted from the Soil Data Federator (Searle et al., 2021) and the Biome of Australian Soil Environments (BASE) contextual data (Bissett et al., 2016). However, the resulting dataset had a reduced spatial coverage and the maps exhibited unrealistic patterns. Hence, we preferred to use all available data and map the proportion of SOC fractions and SOC vulnerability.

The values of SOC proportions were modelled considering their compositional nature (i.e., multivariate data with positive values that sum up to a constant, in the case of SOC fractions 100%). The set of all compositional observations (S^D) is a simplex sample space, a subset of the real space $\mathbb{R}^D$. The ilr-transformation (Egozcue et al., 2003) transposes S^D into multidimensional real space ($\mathbb{R}^{D-1}$), without the collinearity problems associated with other transformations, such as the centered log-ratio transformation (clr). Ilr is based on the choice of an orthonormal basis on the hyperplane in $\mathbb{R}^D$ formed by the clr transformation. The ilr-transformation equation is defined:

$$z_i = ilr(x_i) = \sqrt{\frac{i}{i+1}} \ln\left(\frac{\sqrt[i]{\prod_{j=1}^{i} x_j}}{x_{i+1}}\right), i = 1, 2, \dots, D-1 \quad (1)$$

And the inverse equation is defined as follows (Filzmoser and Hron, 2008):

$$x_i = \frac{\exp(y_i)}{\sum_{i=1}^{D} \exp(y_i)} \; i = 1, 2, \dots, D \quad (2)$$

$$y_i = \sum_{j=i}^{D} \frac{z_j}{\sqrt{j\,(j+1)}} - \sqrt{\frac{i-1}{i}} z_{i=1} \; with \; z_0 = \; z_D = 0 \text{ for } i = 1, 2, \dots, D \quad (3)$$

We applied the ilr-transformation with the *ilr* function of the *compositions* R package (Van Den Boogaart et al., 2022), generating two variables hereafter referred to as ilr1 and ilr2. The predictions (ilr1 and ilr2) were back-transformed into MAOC, POC, PyOC with the *ilrInv* function.

2.6 Coarse fragments

Data on the abundance of coarse fragments (particles > 2 mm) and gravimetric content (% weight) were extracted using the TERN Soil Data Federator (https://esoil.io/TERNLandscapes/Public/Pages/SoilDataFederator/SoilDataFederator.html) managed by CSIRO (Searle et al., 2021). The Soil Data Federator is a web API that compiles soil data from different institutions and government agencies throughout Australia. The abundance (% volume) is assessed visually in the field as part of the soil profile description using standards described in the Australian Soil and Land Survey field Handbook (National Committee on Soil and Terrain, 2009). The abundance of rock fragments per soil horizon on the cut surface of the soil profile was grouped into six categories: very few (0-2 %), few (2-10 %), common (2-20 %), many (20-50 %), abundant (50-90 %) and very abundant (> 90%). The gravimetric content (% mass) is measured in the laboratory as percent mass of coarse fragments (particles > 2 mm) from the whole soil. Here, we take the profile surface abundance of coarse fragments as a proxy for

https://doi.org/10.5194/bg-2022-207
Preprint. Discussion started: 28 October 2022

volumetric coarse fragments (CF_{Vol}). The data was cleaned and processed to exclude duplicates and wrong data entries (e.g., missing values). The observations of CF_{Vol} (%) were converted into GlobalSoilMap depth intervals with the *slab* function of the *aqp* R package (Beaudette et al., 2022), assigning the most probable class to each depth interval. The gravimetric coarse fragments were also standardized to the GlobalSoilMap depth intervals with equal-area quadratic splines (Bishop et al., 1999). Observations of gravimetric coarse fragment content (CF_{Mass}) were transformed into volumetric with Eq.(4):

$$CF_{Vol}\ (\%) = \frac{Vol_{CF}}{Vol_{WhSoil}} \frac{Mass_{CF} / \rho_{CF}}{Mass_{WhSoil} / \rho_{WhSoil}} = \frac{CF_{Mass} \times \rho_{WhSoil}}{\rho_{CF}} \quad (4)$$

where ρ_{WhSoil} is the bulk density prediction for bulk soil from SLGA (Viscarra Rossel et al., 2015), ρ_{CF} is assumed to be 2.65 g cm^{-3} (Hurlbut and Klein (1977) in Mckenzie et al. (2002)) and CF_{Vol} is the volumetric coarse fragment content (continuous),which was assigned to the corresponding class. This resulted in CF_{Vol} observations for 110,308 locations (Figure 3).

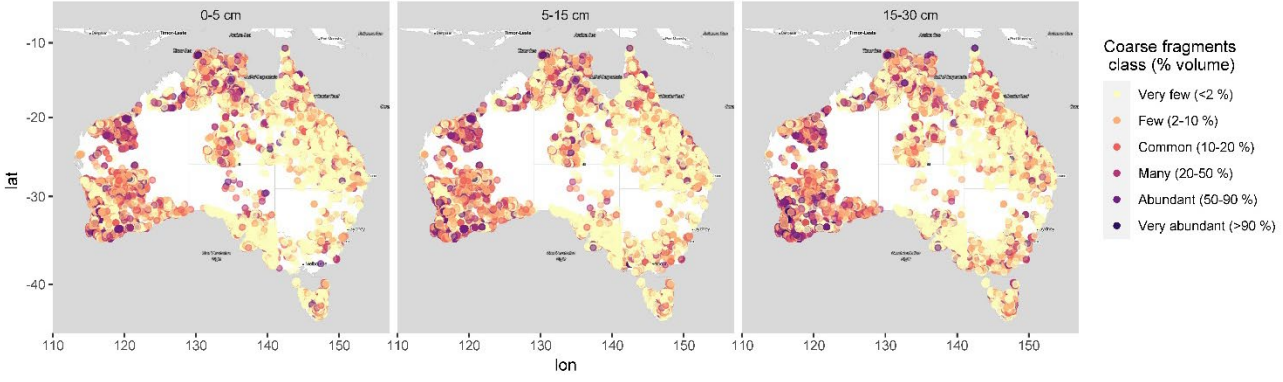

Figure 3:Calibration data on coarse fragments (% volume) classes for the 0-5, 5-15, 15-30 cm depth intervals.

2.7 Environmental covariates

We selected 61 spatially-exhaustive covariates (90 m grid cell size) for Australia made available by TERN, describing soil-forming factors and soil properties (Table 2), to calibrate *scorpan* models (Mcbratney et al., 2003). A scorpan model establishes quantitative relationships between soil properties or classes and other soil properties (*s*), climate (*c*), organisms (*o*), relief (*r*), parent material (*p*), age (*a*), and spatial position (*n*), i.e., *soil = f (s,c,o,r,p,a,n)* (McBratney et al., 2003). We used the soil properties of clay and sand content for each GSM layer due to the relevant role of soil texture in SOC stabilization. We selected 15 climatic covariates since climate is a relevant driver of SOC storage from the global to subregional scale (Wiesmeier et al., 2019), influencing both the SOC decomposition and the C input into the soil. The organisms factor was represented by 22 covariates related to net primary productivity (e.g., Normalized Difference Vegetation Index (NDVI), enhanced vegetation index (EVI)) and vegetation type which influence the C allocation patterns, quantity and pathways of C input (e.g.,

https://doi.org/10.5194/bg-2022-207
Preprint. Discussion started: 28 October 2022

aboveground vs. belowground). Long-term average NDVI calculated with Landsat 5 surface reflectance data was processed with Google Earth Engine. Eight relief covariates were surrogates for elevation, water flow, erosion processes, and sediment transport and accumulation, derived from the 3-second Shuttle Radar Topographic Mission (SRTM) (Farr et al., 2007). Gamma radiometrics, total magnetic intensity and weathering intensity index (Wilford, 2012a) were used as proxies for parent material and age. Gamma radiometrics inform on regolith's mineralogy and surface geochemistry. The concentrations and ratios of three radioelements (potassium (K), thorium (Th), uranium (U)) are indicators of the lithology and degree of weathering (Wilford and Minty, 2007). The weathering intensity index map (Wilford, 2012) was generated from field-based data on the degree of bedrock weathering and multivariate analysis using gamma radiometrics and relief covariates as predictors.

The covariates were void-filled by a combination of plane fitting and inverse distance weighting. The plane fitting method was used to compute the average value of the neighbouring pixels, and otherwise an inverse distance weighting algorithm with default parameters was applied when the error in the plane fitting was large. This is the default implementation from ArcGIS software 10.5.

[Table 2 is at the end of the manuscript]

2.8 Modelling SOC fractions, SOC vulnerability and coarse fragments

Quantile regression forests (Meinshausen, 2006) is a generalization of the popular machine-learning algorithm random forests (Breiman, 2001). Random forests is based on an ensemble of regression trees. Each decision tree is fitted on a bootstrap sample of the original data. Further randomness is incorporated in each individual regression tree by selecting a subset of variables in each node for which the split is made. Whereas random forests report the mean from the observations allocated in each final node, quantile regression forests keeps all values (Meinshausen, 2006), thus estimates of conditional quantiles can be made (Meinshausen, 2006). In DSM, quantile regression forests was applied previously by Vaysse and Lagacherie (2017).

We fitted quantile regression forest models for ilr1, ilr2, and Vp by GSM depth interval with the following settings: ntree = 500 (number of trees), default values of nodesize = 5 (minimum number of observations in terminal nodes) and mtry = 7 (number of predictor variables subset as candidates to make the split at each node). The models were calibrated with the *ranger* package (Wright and Ziegler, 2017) for the R environment. We fitted probability random forest models for coarse fragments (Malley et al., 2012), setting nodesize = 10. In probability random forest models, each tree predicts the class probability for each sample, and these are averaged for the forest probability estimate. The models were evaluated with 10-fold cross-validation. Variable importance was calculated with permutation (Breiman, 2001) on models fitted with 5000 trees and all observations. After the regression trees are constructed, the values of a variable of interest are randomly permuted and the error for the out-of-bag data is estimated. The variable importance is given by the percent increase in error compared with the out-of-bag predictions leaving all variables intact.

We checked the spatial structure of the regression model residuals with cross- and auto- variograms. The spatial cross-correlation was somewhat important at a short range (approximately 20 km) for the 15-30 cm depth interval, but with a high

https://doi.org/10.5194/bg-2022-207
Preprint. Discussion started: 28 October 2022

nugget-to-sill ratio in the fitted variogram models. For the 0-15 cm and 5-15 cm depth, only the residuals of ilr2 had some spatial structure. Overall, we considered the spatial structure of the residuals negligible for the effects of mapping at the continental scale, and hence modelled the spatial distribution of SOC fractions with quantile regression models only.

For mapping, the expected mean values of the SOC fractions, quantile regression forest models for ilr1 and ilr2 were fitted with all available observations, predicted at 90 m resolution and back-transformed into MAOC, POC and PyOC. Similarly, the mean and prediction interval for Vp were predicted with a quantile regression forest model fitted with all observations, setting the 95th and 5th percentiles as prediction interval limits at a 90% confidence level. The prediction intervals for the SOC fractions were calculated from the full conditional probability distributions of ilr1 and ilr2 inferred from the quantile regression forest models. In the model cross-validation, for each observation, a set of 500 values was generated with simple random sampling with replacement from both ilr1 and ilr2 models. Each of the 500 pairs was back-transformed into proportions of MAOC, POC and PyOC (% of SOC). The lower and upper prediction interval limits were calculated as the 5th and 95th percentiles from the empirical distribution of the 500 values of the SOC fractions. For mapping, we used 100 simulations instead of 500 to reduce the computational time. We also mapped the probability of each CF_{vol} class at 90 m resolution.

2.9 Validation statistics

Model performance was assessed with a random 10-fold cross-validation for the ilr-variables, back-transformed SOC fractions predictions and Vp. The validation statistics included the root mean square error (RMSE), the bias or mean error (ME), the coefficient of determination (R^2), and Lin's concordance correlation coefficient (ρ_c) (Lin, 1989). For variable z at a location s_i, the validation statistics are calculated as:

$$RMSE = \sqrt{\frac{1}{n}\sum_{i=1}^{n}\left(z(s_i) - \hat{z}(s_i)\right)^2} \quad (5)$$

$$ME = \frac{1}{n}\sum_{i=1}^{n} z(s_i) - \hat{z}(s_i) \quad (6)$$

$$R^2 = 1 - \frac{\sum_{i=1}^{n}\left(z(s_i) - \hat{z}(s_i)\right)^2}{\sum_{i=1}^{n}(z(s_i) - \bar{z})^2} \quad (7)$$

$$\rho_c = \frac{2\rho\sigma_{\hat{z}}\sigma_z}{\sigma_{\hat{z}}^2 + \sigma_z^2 + \left(\bar{\hat{z}} - \bar{z}\right)^2} \quad (8)$$

where $z(s_i)$ and $\hat{z}(s_i)$ are observed and predicted values of z at the location s_i $(i = 1, \ldots, n)$, $\bar{z}$ and $\bar{\hat{z}}$ are the means of the observed and predicted values, respectively, σ_z^2 and $\sigma_{\hat{z}}^2$ are their respective variances, and ρ is the correlation between predicted and observed values. The concordance evaluates both the accuracy and the precision of the prediction, it can range between −1 and 1, and a value closer to 1 indicates a better agreement between predictions and observations.

We assessed the validity of the uncertainty estimates with the prediction interval coverage probability (PICP) (Shrestha and Solomatine, 2006). The PICP is calculated as:

$$PICP = \frac{count(LPL_i < z(s_i) < UPL_i}{n}\, x\, 100\,, \quad (9)$$

https://doi.org/10.5194/bg-2022-207
Preprint. Discussion started: 28 October 2022

where *n* is the number of observations, and the numerator the counts that an observation $z(s_i)$ fits within its prediction interval limits. If the prediction uncertainty was correctly estimated, for example a 90% confidence level should have a PICP value close to 90% (approximately 90% of the observed values fall within the 90% prediction interval).

The CF_{vol} models were validated with 10-fold cross-validation, assigning the class with the highest probability to each observation prediction. Using the predicted and observed class values, we computed an error matrix. The error matrix is a two-way contingency table composed of the observed and predicted class, for all points within the validation dataset. From the error matrix, we calculated kappa indices: overall accuracy, user's accuracy, producer's accuracy.

The overall accuracy is the fraction of locations correctly classified. It is calculated as:

$$p = \sum_{i=1}^{U} N_{UU} / N \ , \quad (10)$$

where *U* is the total number of classes. The user's accuracy represents the fraction of the class u that is correctly classified (i.e. mapped class *u* in the validation dataset is also observed as class *u*):

$$p_u = \frac{N_{uu}}{N_{u+}} \quad (11)$$

Producer's accuracy is similar to the user's accuracy but is calculated on the columns marginal or the error matrix. It is the fraction of observations *u* for which the prediction is also class *u*. It is obtained as follow:

$$r_u = N_{uu}/N_{+u} \quad (12)$$

For more information on kappa statistics for evaluating map accuracy we refer to Congalton (1991) and Brus et al. (2011).

2.10 Mapping SOC fraction stocks

The expected SOC fraction density for each GSM depth interval *i* was calculated with the following equation, using the map of TOC concentration from v1.2.SLGA (Wadoux et al., 2022), bulk density for the whole soil (Viscarra Rossel et al., 2015), and volumetric coarse fragments:

$$SOC_{fraction\ i\ density}\ (Mg\ C\ ha^{-1}\ cm^{-1}) =$$

$$SOC_{fraction\ i}\left(\frac{mg\ C_{SOC\ fraction\ i}}{mg\ C}\right)\ x\ TOC\ \left(\frac{mg\ C}{g\ soil{<}2\ mm}\right)\ x\ Bulk\ density_{whole}\left(\frac{g\ soil}{cm^3}\right)\ \text{x}\ (1 - Coarse\ Fragments_{vol}\ (\%/100))\left(\frac{soil{<}2\ mm}{g\ soil}\right)\ x\ correction\ units\ \left(\frac{10^8\ cm^2}{ha}\ \frac{Mg}{10^9\ mg}\right) \quad (13)$$

$$Coarse\ Fragments_{vol} = \sum_{u=1}^{6} CF\ probability_u \times CF\ mid_u \quad (14)$$

where $CF\ probability_u$ is the predicted probability and $CF\ mid_u$ the midpoint of the CF_{vol} class *u*. The SOC stock density may be overestimated, especially in soils with high content of rock fragments, due to using the bulk density of whole soil and not of fine soil (Poeplau et al., 2017). We then calculated the SOC fraction stocks for the 0-30 cm depth interval using the median predictions of soil thickness (Malone and Searle, 2020) as a constraint in areas with shallow soils (< 30 cm). We explored differences among SOC fraction stocks (Mg C ha^{-1}) by biome and land use (natural or agriculture) by taking a regular sample of 500,000 pixels across Australia.

https://doi.org/10.5194/bg-2022-207
Preprint. Discussion started: 28 October 2022

The uncertainty of the SOC fraction density for each GSM depth interval was estimated with simulations. We generated a sample of 500 values from the conditional probability distributions of ilr1 and ilr2 and back-transformed those into proportions of MAOC, POC and PyOC (% of SOC). Similarly, we generated a sample of 500 TOC values with the quantile regression model. To account for the uncertainty of the coarse fragment volume, we generated a sample of 500 values where: 1) the number of samples within each CF_{Vol} class was proportional to the predicted class probability, and 2) assuming a continuous uniform distribution within each class. The sample for bulk density was generated assuming a normal distribution, where the standard deviation was calculated from the prediction interval limits, sd =UPL – LPL / 2 x z, with z-score = 1.64 for a 90% prediction interval. We calculated the SOC fraction density for each simulation and calculated the mean and upper and lower prediction interval limits with the 95th and 5th percentiles.

We performed a variance-based, global sensitivity analysis on every pixel to identify which variables account most for the uncertainty of SOC fractions' density and how they vary spatially. We calculated the first-order and total effects Sobol's sensitivity indices (Saltelli et al., 2008). The first-order sensitivity index S_i represents the main effect contribution of each input factor X_i (SOC fraction %, TOC, CF_{vol}, and bulk density) on the variance of the output of model Y (SOC fraction density). It is calculated as the quotient between the variance of the conditional expectation of the output with respect to an input factor, and the the unconditional variance of the output (Saltelli et al., 2008). S_i ranges between 0 and 1, and a high value indicates that factor X_i is an important contributor to the variance of the output (if we knew the true value of X_i we would significantly reduce the variance of Y). The total effect index S_{Ti} includes nonadditive features of the model, by accounting for the first-order effect of X_i and its interactions with other factors on the variance of Y. When S_{Ti} is close to 0, the factor is non-influential on the model output variance. A comprehensive explanation of the variance-based methods for global sensitivity analysis can be found in Saltelli et al. (2008). We calculated the indices with the method by Martinez (2011), with the function sobolmartinez of the sensitivity package in R (Iooss et al., 2021).

3 Results

3.1 Variation of the proportions of SOC fractions with depth and biome

The boxplots of the SOC fraction calibration data showed that most of the TOC was found in the MAOC fraction with a mean (±standard deviation) of 58.8% ± 17.5%, whereas 28.2% ± 17.5% of TOC was PyOC and 13.1% ± 11.1% was POC. The allocation of TOC into the MAOC fractions increased with depth (Figure 4), with a mean (±standard deviation) of 56% ± 17%, 59% ± 17% and 62% ± 18% at 0-5 cm, 5-15 cm and 15-30 cm respectively. Conversely, the proportion of SOC stored as POC decreased with depth, from 15% ± 11% and 13% ± 11% in the top 0-5 cm and 5-15 cm to 11% ± 11% at 15-30 cm. The percentage of SOC in the PyOC fraction remained relatively constant with depth, with values around 29% ± 17% (Figure 4). Hence, in average, carbon vulnerability decreased with depth, with Vp = 1.4 ± 98.6 at 0-5 cm, Vp = 0.5 ± 29.7 at 5-15 cm and Vp = 0.2 ± 3.4 at 15-30 cm.

https://doi.org/10.5194/bg-2022-207
Preprint. Discussion started: 28 October 2022

395

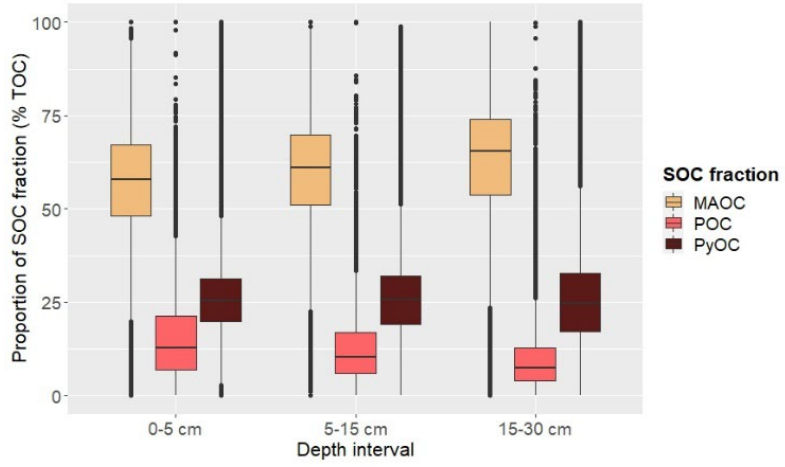

Figure 4: Distribution of total organic carbon (TOC) among three soil organic carbon (SOC) fractions in the calibration dataset. Mineral-associated SOC (MAOC), particulate organic carbon (POC), and pyrogenic organic carbon (PyOC).

400 The distribution of TOC among fractions showed similar patterns across biomes (MAOC >> PyOC > POC), except for montane grasslands and shrublands where 67% of TOC was stored as PyOC while only 27% was stored as MAOC (Table 3 and Figure S2). However, there were only 160 observations located in this biome. The proportion of TOC as POC was greater in Mediterranean forests and scrub, temperate forests, and tropical and sub-tropical forests. In Mediterranean systems, the proportion of MAOC was around 10% less than across the other biomes, (excluding montane grasslands), whereas the smallest
405 proportion of PyOC was found in tropical and subtropical forests. Hence, the Vp was highest in the Mediterranean biome followed by temperate forests, and tropical and subtropical forests, decreasing with depth across all biomes (Table 3).

Table 3: Summary statistics, mean (±standard deviation) of SOC fractions and SOC vulnerability (Vp) by biome. N: number of observations. Mineral-associated SOC (MAOC), particulate organic carbon (POC), and pyrogenic organic carbon (PyOC).

Biome	Depth	N	MAOC (% SOC)	POC (% SOC)	PyOC (% SOC)	Vp
Montane Grasslands and Shrublands	0-5 cm	160	26.0 ± 9.4	7.1 ± 6.7	66.9 ± 14.3	0.08 ± 0.1
	5-15 cm	160	26.7 ± 10.3	6.1 ± 5.5	67.2 ± 14.8	0.07 ± 0.1
	15-30 cm	152	27.6 ± 13.0	4.8 ± 4.1	67.7 ± 16.3	0.05 ± 0.1
Temperate Broadleaf & Mixed Forests	0-5 cm	2865	54.4 ± 10.2	20.6 ± 8.3	25.0 ± 8.1	2.49 ± 118.3
	5-15 cm	2871	58.4 ± 10.3	15.6 ± 6.8	26.0 ± 8.5	0.64 ± 23.8
	15-30 cm	2722	64.2 ± 11.1	10.3 ± 6.7	25.5 ± 9.8	0.26 ± 7.2
	0-5 cm	750	57.6 ± 18.0	11.5 ± 7.1	31.0 ± 20.5	0.14 ± 0.1

https://doi.org/10.5194/bg-2022-207
Preprint. Discussion started: 28 October 2022

Temperate Grasslands, Savannas & Shrublands	5-15 cm	762	60.5 ± 19.1	9.2 ± 6.0	30.5 ± 20.5	0.11 ± 0.1
	15-30 cm	703	61.8 ± 20.1	7.6 ± 6.8	30.7 ± 21.3	0.09 ± 0.1
Mediterranean Forests, Woodlands & Scrub	0-5 cm	4671	49.2 ± 17.0	20.3 ± 13.8	30.6 ± 20.3	2.46 ± 146.3
	5-15 cm	4695	51.7 ± 18.3	17.8 ± 13.7	30.5 ± 20.0	0.97 ± 48.5
	15-30 cm	4229	54.8 ± 21.0	15.7 ± 15.3	29.5 ± 20.7	0.28 ± 1.42
Deserts & Xeric Shrublands	0-5 cm	2427	65.3 ± 16.2	8.3 ± 6.7	26.4 ± 17.6	0.10 ± 0.1
	5-15 cm	2421	66.1 ± 16.5	7.5 ± 6.6	26.5 ± 17.7	0.09 ± 0.1
	15-30 cm	2187	67.0 ± 17.0	6.7 ± 7.3	26.3 ± 17.7	0.08 ± 0.2
Tropical & Subtropical Grasslands, Savannas & Shrublands	0-5 cm	3283	61.5 ± 13.9	10.0 ± 7.1	28.5 ± 14.8	0.12 ± 0.1
	5-15 cm	3236	63.8 ± 14.5	8.6 ± 6.2	27.6 ± 15.3	0.10 ± 0.1
	15-30 cm	2851	67.3 ± 15.0	7.4 ± 6.3	25.3 ± 15.4	0.09 ± 0.1
Tropical & Subtropical Moist Broadleaf Forests	0-5 cm	242	61.9 ± 18.7	18.4 ± 11.4	19.7 ± 20.1	0.27 ± 0.4
	5-15 cm	243	65.1 ± 18.7	16.8 ± 10.4	18.2 ± 19.8	0.24 ± 0.4
	15-30 cm	234	70.1 ± 18.3	14.6 ± 9.6	15.2 ± 18.4	0.20 ± 0.4

3.2 Cross-validation statistics for SOC fractions

The cross-validation statistics indicated that both ilr-fractions models had similar RMSE and bias, although the R^2 and ρ_c were better for ilr2 than ilr1. Model performance indices decreased with depth but were overall good, with $R^2 \geq 0.54$ for ilr1 and $R^2 \geq 0.68$ for ilr2. Similarly, the concordance coefficients indicated good agreement between predictions and observations, with $\rho_c \geq 0.70$ for ilr1 and $\rho_c \geq 0.81$ for ilr2. The uncertainty was somewhat underestimated (Table 4) but close to a PICP of 90%. The cross-validation of the back-transformed SOC fractions indicated that the concordance coefficient and R^2 followed the trend PyOC > MAOC > POC (Table 4). Contrarily, the RMSE was greatest for MAOC with values between 8.4 % and 10.4 %, and were somewhat smaller for PyOC and POC, between 8 % and 6 %. SOC fractions predictions had a small bias, with an average underprediction of MAOC and overprediction of POC and PyOC. The accuracy plots (Supplementary material Figure S3) indicate that the uncertainty was overestimated for MAOC and PyOC, and underestimated for POC, for all probability intervals, although the uncertainty was adequately estimated for the 90% prediction interval (Table 4). Cross-validation statistics for SOC vulnerability were worse than for the SOC fractions, with R^2 ranging between 0.39 to 0.56 and concordance coefficient between 0.58 and 0.72, which is possibly due to some extreme values in the calibration dataset. A PICP around 86% indicates that the uncertainty was somewhat underestimated.

https://doi.org/10.5194/bg-2022-207
Preprint. Discussion started: 28 October 2022

Table 4: Cross-validation statistics for ilr1, ilr2, mineral-associated SOC (MAOC), particulate organic carbon (POC), pyrogenic organic carbon (PyOC) and SOC vulnerability (Vp) by depth interval. Mean error (ME), root mean squared error (RMSE), coefficient of determination (R^2), Lin's concordance correlation coefficient (ρ_c) and prediction interval coverage probability (PICP).

Ilr-transformed SOC fractions	Depth	ME	RMSE	R^2	ρ_c	PICP (%)
	0-5 cm	-0.01	0.45	0.60	0.75	85.4
ilr1	5-15 cm	-0.01	0.42	0.63	0.77	86.1
	15-30 cm	-0.01	0.56	0.54	0.70	85.8
	0-5 cm	0.01	0.46	0.73	0.84	86.3
ilr2	5-15 cm	0.01	0.47	0.74	0.85	86.5
	15-30 cm	0.00	0.58	0.68	0.81	86.4
	0-5 cm	0	0.21	0.39	0.58	86.1
Vp	5-15 cm	0	0.17	0.56	0.72	86.3
	15-30 cm	0	0.21	0.56	0.72	86.3
Soil property	Depth	ME (%)	RMSE (%)	R^2	ρ_c	PICP (%)
	0-5 cm	1.18	8.42	0.74	0.85	95.1
MAOC	5-15 cm	1.27	8.84	0.73	0.85	94.9
	15-30 cm	2.00	10.35	0.68	0.82	94.9
	0-5 cm	-0.88	6.58	0.67	0.80	84.7
POC	5-15 cm	-0.83	6.20	0.65	0.79	85.5
	15-30 cm	-1.24	7.06	0.59	0.74	85.2
	0-5 cm	-0.31	7.72	0.80	0.89	93.7
PyOC	5-15 cm	-0.46	7.92	0.79	0.89	93.7
	15-30 cm	-0.77	8.78	0.76	0.87	94.0

3.3 Cross-validation statistics for coarse fragment classes

The overall accuracy of predicting coarse fragments classes was 67% for the 0-5 cm, 66% for the 5-15 cm, and 63% at the 15-30 cm depth interval. The Kappa statistics were 0.39, 0.38, and 0.37, respectively, which indicate some agreement. The producer's accuracy was around 90 % for the 'very few' class across the three depths, but the omission error was significant for the remaining classes, especially for 'common' and 'very abundant' with values around 15 %. The user's accuracy was smaller than 50% for the classes 'few', 'common', and 'many' coarse fragments but improved somewhat for 'very abundant', 'abundant', and 'few' (Table 5). The confusion matrices are provided in the Supplementary material (Table S1-S3).

https://doi.org/10.5194/bg-2022-207
Preprint. Discussion started: 28 October 2022

Table 5: Cross-validation statistics for classification of coarse fragments (% volume).

	Depth	Very few (< 2 %)	Few (2-10 %)	Common (10-20 %)	Many (20-50 %)	Abundant (50-90 %)	Very abundant (> 90%)
Producer's accuracy (%)	0-5	93	39	17	35	22	15
	5-15	92	40	16	34	21	12
	15-30	92	38	13	31	39	8
User's accuracy (%)	0-5	76	47	42	44	58	56
	5-15	74	47	43	43	53	63
	15-30	71	46	42	43	53	52

3.4 Variable importance for predicting proportions of SOC fractions and coarse fragments

The environmental covariates important for both ilr1 and ilr2 models were parent material and climate, whereas relief and organisms were secondary factors (Figure 5). The rank of the 10 most important variables indicates that parent material, soil properties and relief were more relevant for ilr1, especially gravity, gamma radiometrics K, clay and elevation (DEM), whereas for ilr2 the importance of gamma radiometrics variables and gravity was more patent for the depth intervals 5-15 cm and 15-30 cm. On the contrary, climate variables were more critical for ilr2 models, especially precipitation seasonality (PTS1 and PTS2), potential evaporation (EPA and EPX), and annual temperature (TNM and TXM), while annual temperature range (TRA) was more important for the ilr1 model. Amongst the relief covariates, DEM, topographic wetness index (TWI) and roughness were the most relevant variables for both ilr1and ilr2. Non-photosynthetic vegetation and mean EVI were the only covariates representing the soil-forming factor organisms with some importance in the models. The most significant variables predicting the distribution of coarse fragments were gamma radiometrics and other proxies of parent material (Th, U, total dose, and ratio Th/K), followed by some covariates of climate (EPX, TRA), and relief (roughness, slope, DEM) (Figure 6).

https://doi.org/10.5194/bg-2022-207
Preprint. Discussion started: 28 October 2022

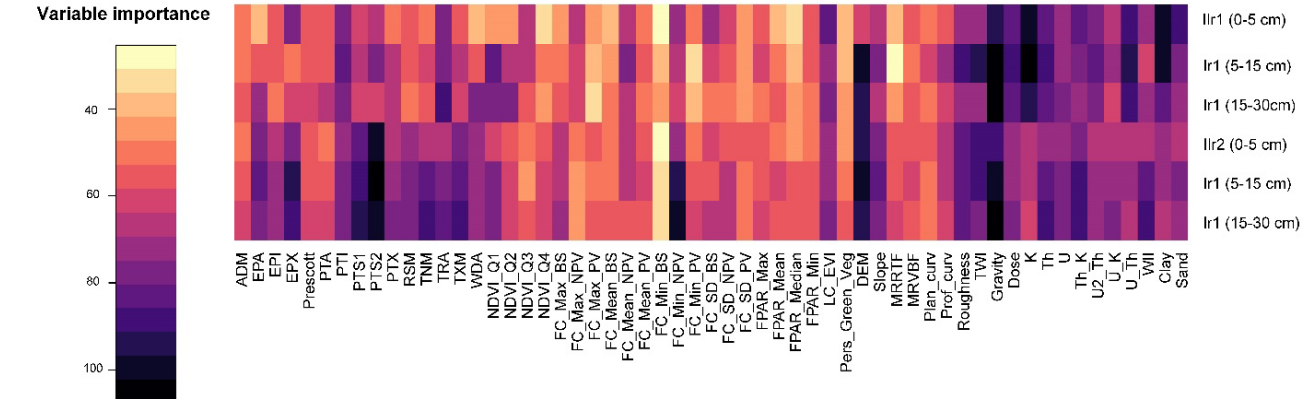

455 **Figure 5: Variable importance of random forest models for predicting ilr-transformed SOC fractions. Variable importance was calculated from permutation as per Breiman (2001).**

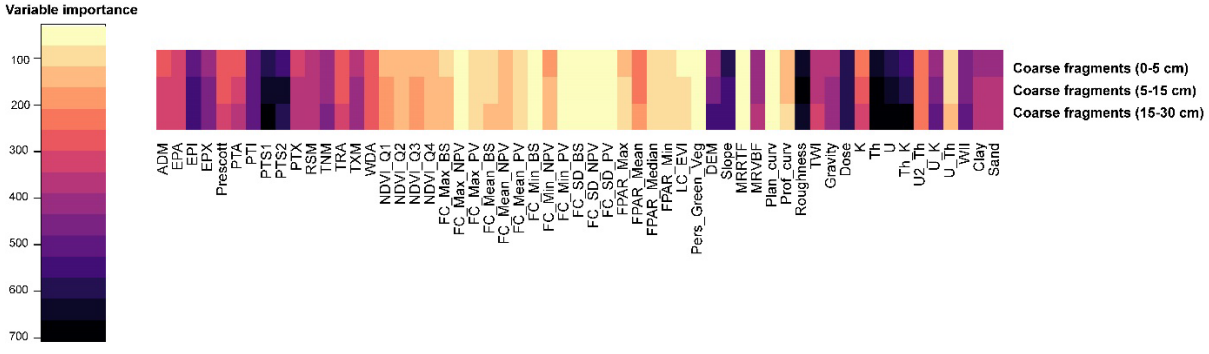

Figure 6: Variable importance of random forest probability models for coarse fragments classes. Variable importance was estimated
460 **with Gini index impurity (Sandri and Zuccolotto, 2008).**

3.5 Maps of SOC fraction proportions, SOC vulnerability and coarse fragments

The spatial predictions of SOC fractions allocated most of SOC to the MAOC fraction across most of Australia (Figure 7.a and Figures S4-S6). The POC proportion was greater in the Mediterranean and temperate areas along the coast and north
465 Queensland. There were three main regions with a high proportion of PyOC: in the north-west around Prince Regent River and Dampier Peninsula, in the west south of the Gascoyne River, and in some parts of the south-centre, e.g., east of Lake Frome. These predictions are likely driven by some calibration data with high PyOC values at these locations (Figure 2). The prediction intervals for the SOC fractions were wide (Figures S4-S6), although based on the accuracy plots (Figure S3) was estimated relatively well at the 90% confidence level. Therefore, SOC vulnerability was higher in areas with Mediterranean
470 and temperate climate and in the centre-east (Figure 7.b). The latter is likely an artifact since that area is largely occupied by

https://doi.org/10.5194/bg-2022-207
Preprint. Discussion started: 28 October 2022

salt lakes (Kati-Thanda /Lake Eyre) and the Strzelecki desert. The coarse fragment class with highest probability across Australia was "very few" (< 2 %), and the estimated volume of coarse fragments was higher in the west and north-west Australia as well as along the Great Divide (Figures S7-S9).

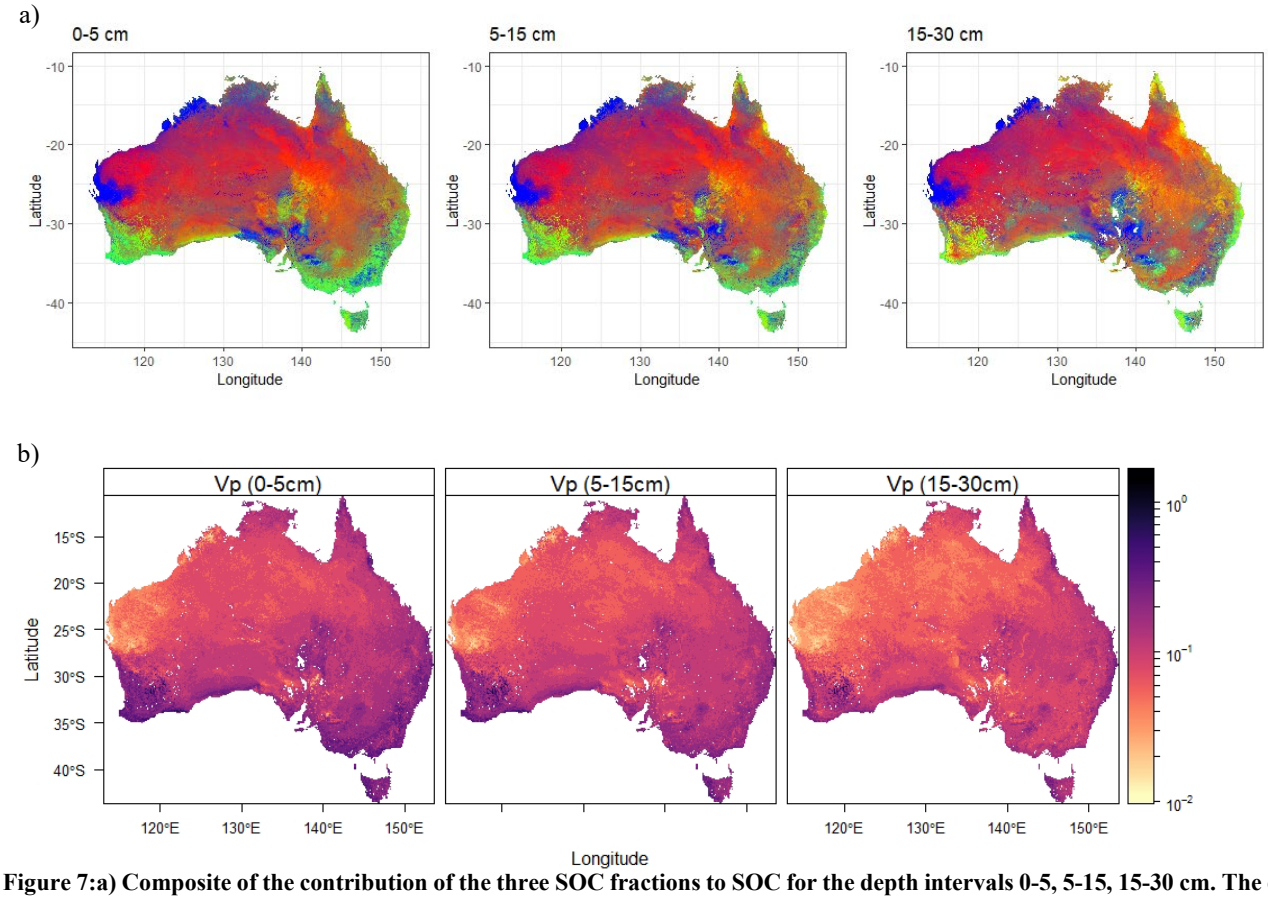

Figure 7:a) Composite of the contribution of the three SOC fractions to SOC for the depth intervals 0-5, 5-15, 15-30 cm. The colours indicate the dominant fractions with MAOC in red, POC in green and PyOC in blue. b) SOC vulnerability for the three depth intervals. SOC vulnerability is in the log10 scale for better differentiation.

3.6 SOC fraction density and sensitivity analysis

The spatial patterns of SOC fractions density are mainly determined by the spatial gradient in TOC concentration. Thus, irrespective of the dominant fraction, SOC density follows a climatic gradient and is higher in the south-west, east, Tasmania, and some regions in north Australia (Figures S10-S12). PyOC density was predicted higher along the Snowy Mountains, as the proportion of PyOC in montane grasslands and shrublands in the calibration dataset was around 67% (Table 3) and the TOC concentration was high (Figure S10). POC density was higher in southwestern Australia, east of Tasmania and in the

https://doi.org/10.5194/bg-2022-207
Preprint. Discussion started: 28 October 2022

485 southeast and east. MAOC density showed similar patterns and had higher values than POC. Ultimately, the SOC fraction stocks in the 0-30 cm (Figure 8) were not high in the east of Tasmania because these are peat soils, and the estimated median soil thickness was estimated for mineral soils. Similarly, the SOC stocks in the Snowy mountains were constrained by the shallow soil thickness. The total stock of SOC fractions for Australia (0-30 cm) were 12.7 Pg MAOC, 2 Pg POC and 5.1 Pg PyOC. While we have calculated the uncertainty of the SOC fractions density (mg C cm^{-3}) by depth interval with simulation
490 (Figures S11-S13) we have not calculated the uncertainty of the total stocks taking into account the uncertainty of soil thickness.

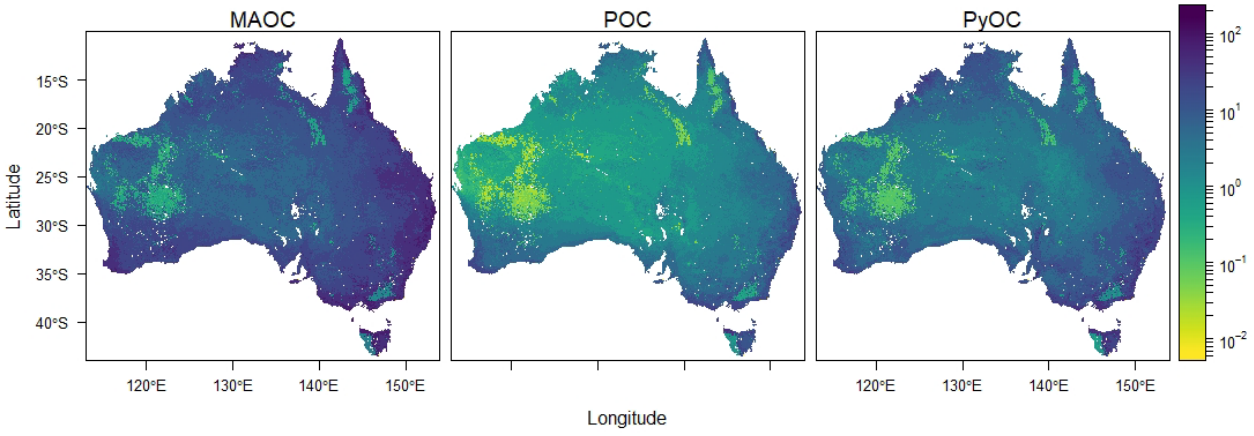

Figure 8:SOC fraction stocks (0-30 cm) (Mg C ha^{-1}). The values are represented in the log10 scale.

495 MAOC stocks were generally higher in tropical and subtropical moist broadleaf forests and temperate broadleaf and mixed forests (Figure 9). In some biomes (temperate and tropical grasslands, savannas and shrublands, and desert and xeric shrublands), MAOC stocks were higher in agricultural soils (which included rainfed and irrigated pastures), than in natural areas. In the Mediterranean biome, MAOC stocks were similar in natural and agricultural regions. POC stocks followed similar trends than MAOC, although in the Mediterranean biome, POC was greater in agricultural soils than in natural areas. Montane
500 grasslands and shrublands had maximum values of PyOC, although the median PyOC stocks were greater in the natural and agricultural temperate biome, followed by tropical and subtropical forests (Figure 9).

https://doi.org/10.5194/bg-2022-207
Preprint. Discussion started: 28 October 2022

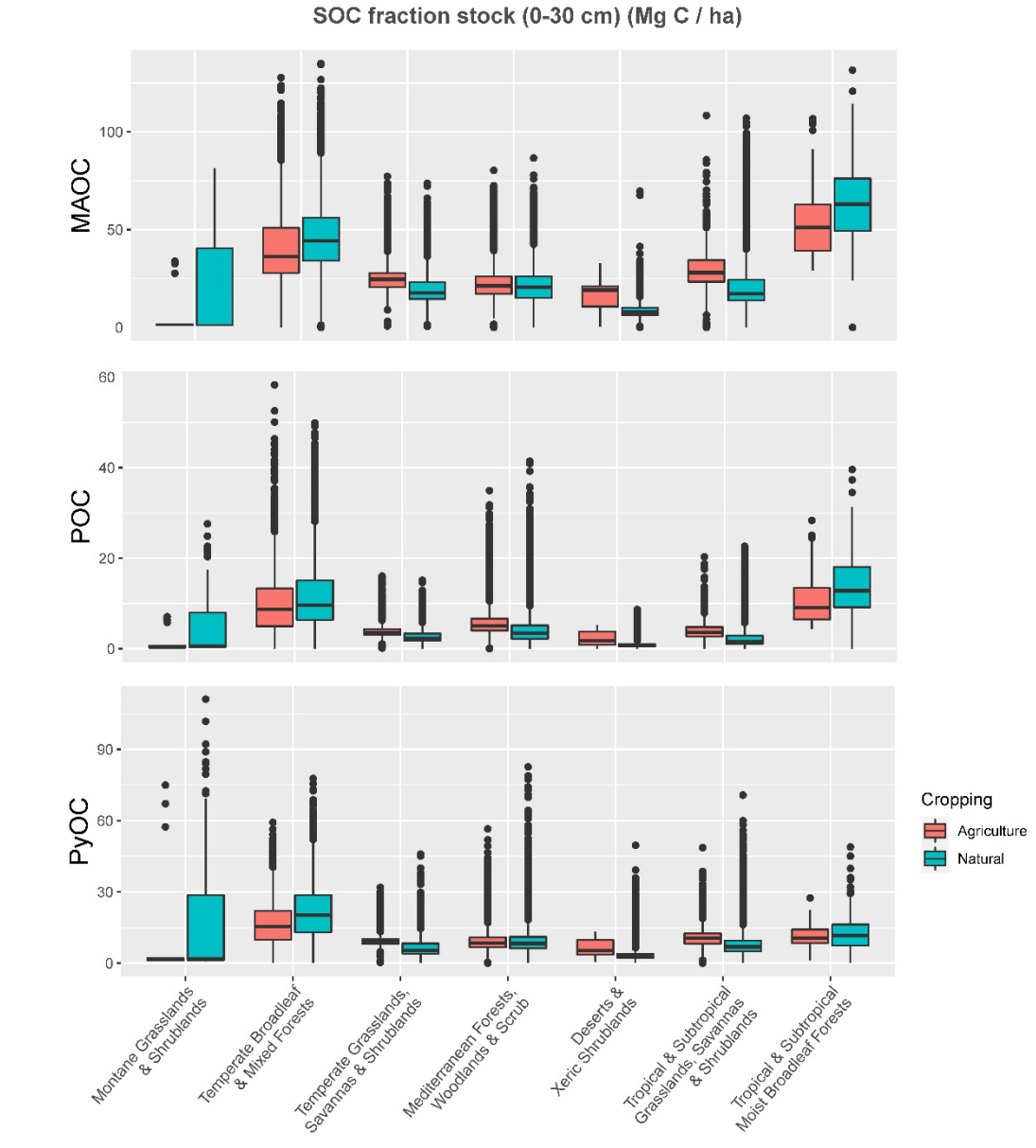

Figure 9: SOC fraction stock (Mg C ha^{-1}) by biome and land use. Mineral-associated SOC (MAOC), particulate organic carbon (POC), pyrogenic organic carbon (PyOC).

505

The two variables with most influence on the uncertainty of SOC fraction density were TOC concentration and SOC fraction % (Figures S14-S19). The total Sobol indices varied spatially depending on the SOC fraction, with TOC being the most relevant in interior areas with smaller SOC stocks, and both variables having similar influence towards the coast in the southern half of the continent. Total Sobol indices show that bulk density was not very influential on the uncertainty of the SOC fraction

https://doi.org/10.5194/bg-2022-207
Preprint. Discussion started: 28 October 2022

density. This may be related to the relatively small prediction interval of the bulk density maps, calculated with bootstrapping (Viscarra Rossel et al., 2015). Coarse fragments also had a small influence as indicated by the small Sobol indices across most of Australia except in zones where a higher volume of coarse fragments had higher probability, e.g., western and northern Australia (Figures S7-S9).

4 Discussion

4.1 Differences in SOC allocation into fractions across biomes

The trend of lower MAOC proportion with increasing sand content was observed across all biomes (Figure 10). Sand content is generally higher in the western half of Australia, coinciding with the Mediterranean and desert biomes, which have a mean (± standard deviation) of 73% ± 14% and 71% ± 10%, respectively, in the calibration dataset. The smaller capacity of coarse-textured soils to stabilize SOC through organo-mineral associations may partly cause the lower proportion of MAOC and higher POC in Mediterranean soils (Figure 9 and Figure 10). Similarly, Doetterl et al. (2015) found that more SOC was stored as POC in arid environments where biochemical weathering is limited, due to a lower capacity for physico-chemical protection. Conversely, around 60% of MAOC can be found in Australian temperate grasslands, savannas and shrublands, 50 % MAOC in Mediterranean forests and woodlands, ~ 54-64% MAOC in temperate forests and 65-65 % MAOC in tropical (Table 3). Sokol et al. (2022) reported a high proportion of MAOC in temperate grasslands (~ 70 %) was due to higher NPP and microbial decomposition favouring MAOC formation. They also found that savannas, temperate and tropical forests had a relatively high proportion of MAOC (~ 64 %), whereas shrublands had a lower proportion of MAOC (~ 42 %). Some differences are possibly explained by a higher percentage of SOC as PyOC in some systems (e.g., montane grasslands, tropical and subtropical savannas), in comparison to two fractions (MAOC and POC) (Sokol et al., 2022), and differences in the definition of biomes.

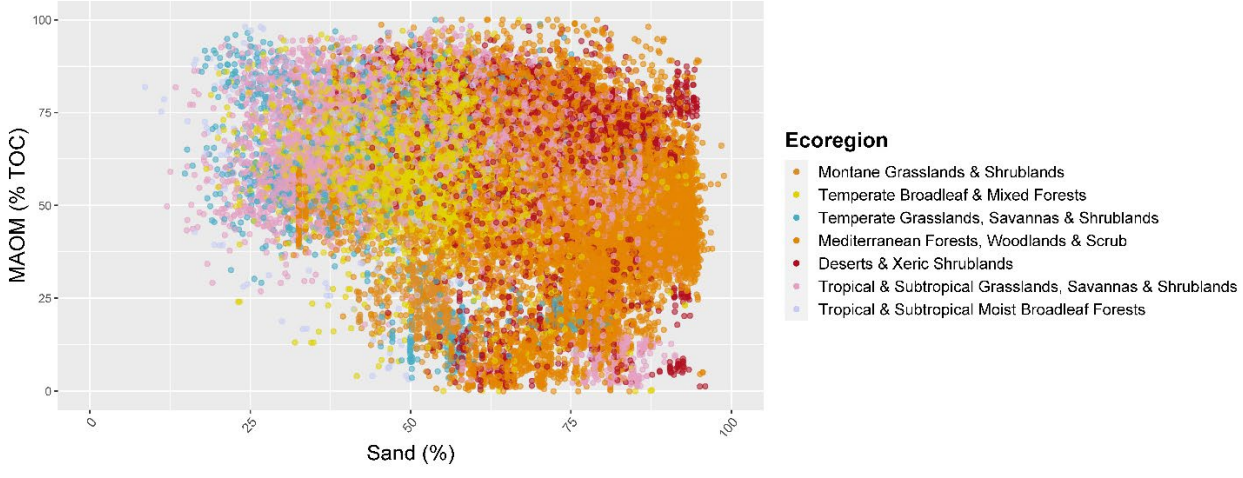

https://doi.org/10.5194/bg-2022-207
Preprint. Discussion started: 28 October 2022

Figure 10: Allocation of SOC into the mineral-associated organic carbon fraction (MAOC) plotted vs. sand content (%) by biome, from calibration data.

4.2 Abiotic and biotic predictors of SOC allocation into SOC fractions at the continental scale

Climate and parent material were the main soil-forming factors for predicting the partition of SOC into fractions in continental Australia. Climate is a major driver of SOC storage (Wiesmeier et al., 2019) and partition into SOC fractions at continental scale (Bui et al., 2009). Climate influences weathering of primary minerals, the development of reactive secondary minerals over long-term pedogenetic processes, and the chemistry of the soil solution, which in turn condition the formation of organo-mineral associations (Kleber et al., 2015). At the same time, climate also controls SOC decomposition rates and input of organic matter through net primary productivity. At the global scale, climate is a major driver of the abundance, persistence, and distribution of SOC among fractions (Heckman et al., 2022), with different effects by fractions and depth. Mean annual temperature had a strong effect on POC. In contrast, the wetness index (ratio of annual precipitation to potential evapotranspiration) had a stronger effect on MAOC, suggesting that under wetter conditions, weathering and increasing reactivity of minerals with depth, together with the downward transport of organic matter, enhances the formation of organo-mineral associations (Kleber et al., 2015). Parent material alone did not have a significant effect on the partition of SOC into MAOC at the global scale, but in interaction with the wetness index (Heckman et al., 2022).

In this study we could not verify the influence of soil geochemistry and mineralogy (metal ions, sesquioxides) on the proportion of SOC fractions due to lack of samples with extensive laboratory analysis. Soil geochemical properties have been found to control SOC storage at continental and regional scales (Doetterl et al., 2015b), and are involved in the stabilisation of SOC with different mechanisms depending on the climatic context and soil pH (Lutzow et al., 2006; Rasmussen et al., 2018). In Australia, soil physico-chemical properties, and particularly extractable iron, were the most important predictors of SOC storage at the continental scale (Li et al., 2020). Multiple soil chemical properties can be estimated fairly well with mid-infrared spectral models (Ng et al., 2022). Therefore, future research could expand on this study by investigating the relationships (and their spatial patterns) between soil chemical properties (exchangeable Ca and Mg, oxalate and dithionite extractable Fe and Al) and MAOC in the context of Australia, where the soil pH is quite acidic even under arid and semi-arid conditions.

Among vegetation variables, only EVI and the fractional cover of non-photosynthetic vegetation were important predictors for the distribution of SOC among fractions. The fraction of non-photosynthetic vegetation may be indicative of the type of C input into the soil (e.g., woody debris), which influences the subsequent decomposition and transformation pathways of organic matter (Cotrufo et al., 2015) and the allocation into SOC fractions (Heckman et al., 2022).

4.3 Vulnerability of SOC fractions to climate change

We estimated the total stock of SOC fractions for Australia (0-30 cm) in 12.7 Pg MAOC, 2 Pg POC and 5.1 Pg PyOC, which give a total of 19.8 Pg SOC. This value is smaller than a previous baseline of SOC stock of 25 Pg SOC for Australian topsoils, but within its prediction interval (19-31.8 Pg C) (Viscarra Rossel et al., 2014). Differences in the total SOC stock may be partly

https://doi.org/10.5194/bg-2022-207
Preprint. Discussion started: 28 October 2022

due to differences in TOC predictions between the previous version of SLGA v1 (Viscarra Rossel et al., 2015; Viscarra Rossel et al., 2014) and the current SLGA v1.2 (Wadoux et al., 2022). Both maps show similar patterns and range of TOC values, and hence differences in SOC fraction and total SOC stock may be mostly caused by differences in the DSM framework (e.g., calculating SOC fraction densities prior to spatialization, accounting or not with coarse fragments, etc.).

Our calculations estimated that about 64% of the total SOC is stored as mineral-associated SOC, which is consistent with other studies at global and continental scales (Heckman et al., 2022). In Australian topsoils, we estimated that only 10% of the SOC stock is stored as POC and 26% as PyOC. POC is generally more responsive than MAOC to management practices and to global change (Rocci et al., 2021). Our PyOC estimate is higher than the world average (14% of SOC (Reisser et al., 2016)) but is consistent with a study in Australia (14-33%, (Lehmann et al., 2008)). Since the 1970s, there is an upward trend in "fire weather" conditions in Australia linked to anthropogenic climate change (Harris and Lucas, 2019), which may modify the proportion and stock of PyOC.

There is great uncertainty about the effects of an increase in temperature on SOC fractions stocks and dynamics. There is large evidence supporting that the temperature sensitivity of decomposition is higher for stable SOC fractions (Conant et al., 2008; Jia et al., 2020) or SOC pools with longer mean residence time (Li et al., 2013), although other studies indicate no differences or opposite trends in sensitivity between SOC fractions (Von Lützow and Kögel-Knabner, 2009). Since most of SOC is stored as MAOC, an increase in MAOC decomposition rates with temperature (when soil moisture is not limiting) may turn some soils into a C source (Li et al., 2013). Contrarily, coarse-textured soils with a lower capacity for physico-chemical protection and a greater proportion of POC may be more vulnerable to SOC loss with an increase in temperature than fine-textured soils (Hartley et al., 2021). Heckman et al. (2022) found a decrease in SOC persistence among all SOC fractions with higher mean annual temperature at the global scale, and a decrease in SOC abundance in free POC in the surface (0-30 cm). But the increase in temperature did not affect the abundance of occluded POC and MAOC, which may be less vulnerable to warming. Similarly, a recent meta-analysis (Rocci et al., 2021) found a reduction of POC (% SOC) with warming, suggesting that soils with higher POC contribution may be more vulnerable to SOC loss. In the case of Australia, this would mean that coarse-textured soils from Mediterranean and temperate ecosystems may be more vulnerable to an increase in temperature.

Other climatic and hydrological conditions linked to climate change may also affect SOC fractions stocks in Australia. Changes in the precipitation regime (e.g., intensity and frequency of droughts, extreme precipitation events and flooding) can affect the SOC fraction stocks by either limiting or enhancing C input into the soil (effects on NPP), as well as modifying decomposition or SOC losses by increased erosion. Rocci et al. (2021) did not find clear effects on the partition of SOC among fractions with an increase in precipitation, although they found a negative tendency for POC and a positive tendency on MAOC. The effect of wind erosion on SOC loss will depend on particle size distribution and soil cover, with vulnerable soils losing 3.6 Mg C ha^{-1} in south-western Australia (Harper et al., 2010). While wind erosion may deplete locally the soil of clay and silt-size particles, and light SOC fractions (light MAOC and light POC), and facilitate mineralization by disruption of aggregates, aeolian transport and deposition of may contribute to SOC enrichment in other regions (Webb et al., 2012). The influence of water erosion on SOC fractions will vary with agricultural practices, with the latter sometimes having a stronger effect on POC than

https://doi.org/10.5194/bg-2022-207
Preprint. Discussion started: 28 October 2022

erosion depending on hillsope position (Zhao et al., 2022). SOC desestabilization and stabilization processes vary along the hillslope with changes in particle size distribution, degree of weathering, and abundance of secondary minerals (Doetterl et al., 2015a).

4.4 Components in the calculation of SOC fraction stocks: priorities for improving their quantification

The maps of total Sobol indices inform which variables are more influential on the uncertainty of SOC fraction densities across Australia, and can guide the priorities for mapping locally, regionally or at a continental scale the different components of SOC fraction stocks. TOC was the main variable of influence for SOC fraction density, and methods for measuring it efficiently and more economically on-farm and at the laboratory are experiencing continuous development. TOC concentration in Australian ecosystems has been underestimated by previous SOC maps in temperate forests (Bennett et al., 2020). It is possible that in this study, the SOC fraction stocks for these ecosystems are a conservative estimate since the random forests models tend to underestimate the high values (Wadoux et al., 2022).

The percentage of TOC in the three fractions was generally the second variable of influence on the uncertainty of SOC fractions density. Still, it could be the most influential variable in areas with moderate to low SOC density. Several sources of error in the SOC fraction predictions were not accounted for in the sensitivity analysis, like the error propagated from the different spectral models or the fact that the fractionation in the original dataset was applied to agricultural soils and some pastures but lack forest soils. There is also an under representation of some biomes and land cover types (e.g., tropical savannas) in the dataset used for fractionation. Ideally, the spectral models could be improved by increasing the representation of different natural ecosystems, which may have very different mechanisms of stabilization.

We used estimates of rock fragment volume in the calculation of SOC fraction stocks, which can overestimate the stocks when the bulk density is for the whole soil instead of that of the fine soil (< 2 mm) (Poeplau et al., 2017). The error due to combining volumetric coarse fragments and bulk density of the whole soil is not captured in the sensitivity analysis. Neglecting the content of coarse fragments can significantly overestimate the SOC fraction stocks in soils with non-negligible stoniness (> 5 %), more than doubling the actual stocks in soils with > 30% rock fragments (Poeplau et al., 2017). We anticipated that the inaccuracy of the coarse fragments' maps and the broad range within each category would contribute significantly to the error and uncertainty in the SOC fraction stocks estimates. This was true in areas with non-negligible stoniness (> 2%), as indicated by the total Sobol indices (Figures S14-S19). However, compared with the distribution among SOC fractions and TOC concentration, coarse fragments were not the most relevant variable influencing SOC fraction density.

Conclusions

SOC fractions are crucial as input for SOC dynamics models. These maps of MAOC, POC and PyOC can be used as input for modelling SOC stocks under different management strategies and identify areas where SOC stocks could be augmented more efficiently (i.e., areas with higher SOC sequestration potential/SOC deficit) (Meyer et al., 2017; Martin et al., 2021). Land

https://doi.org/10.5194/bg-2022-207
Preprint. Discussion started: 28 October 2022

management practitioners could then optimize the spatial allocation of different agricultural practices while maintaining several soil functions and services, mainly food security and climate change mitigation and adaptation.

The main covariates predicting the distribution of SOC among fractions at the continental scale were identified as climate and parent material. Yet, a comprehensive and homogeneous dataset that examines the soil geochemical properties (e.g., exchangeable Ca and Mg, extractable Fe and Al, CEC ascribed to minerals, etc.) controlling SOC stabilisation processes is lacking in Australia. The diversity of climatic and pedological conditions suggests that different mechanisms will control SOC stabilization and dynamics across the continent, as observed in other regions (Rasmussen et al., 2018). The link between mycorrhizal associations (Averill et al., 2014; Jo et al., 2019) and soil microbial community composition (e.g., N_2-fixing organisms), soil stoichiometry and vegetation communities (Bui and Henderson, 2013), and their effects on SOC fractions (Cotrufo et al., 2019) should be further investigated. For example, it is possible that in native ecosystems with higher soil C:N ratio and recalcitrant litter, there may be a high proportion of SOC as POC, whereas the MAOC fraction may not be C-saturated.

The uncertainty on the spatial predictions of SOC fraction stocks was driven mainly by TOC and the proportion of SOC fractions predictions, which in turn rely on spectral predictive models developed with soil samples originating mainly from agricultural soils. However, the sensitivity analysis allows targeting variables that should be prioritised at the local and regional scale to reduce the uncertainties of SOC fraction stock estimates. Future works shall include more efforts into sampling for measuring TOC, fractionation on underrepresented regions, or developing local spectral models for predicting SOC fractions.

Acknowledgments

The authors acknowledge the Sydney Informatics Hub and the use of the University of Sydney's high performance computing cluster, Artemis, that enabled the computations for mapping at 90 m resolution for continental Australia. We also acknowledge the high-performance computing facilities from CSIRO that were used for mapping at 90 m resolution the SOC fraction densities. Some data was sourced from Terrestrial Ecosystem Research Network (TERN) infrastructure, which is enabled by the Australian Government's National Collaborative Research Infrastructure Strategy (NCRIS). This work was partly funded by the Terrestrial Ecosystem Research Network (TERN), an Australian Government NCRIS-enabled project. MRD, AMJCW BM and AMcB acknowledge support from the Research Portfolio at the University of Sydney. AMcB acknowledges support via the Australian Research Council's Laureate Program entitled 'A calculable approach to securing Australia's soil'

Data availability

The observed data on total organic carbon and coarse fragments are publicly available in their majority from the Soil Data Federator (https://esoil.io/TERNLandscapes/Public/Pages/SoilDataFederator/SoilDataFederator.html). The covariate data is available at https://esoil.io/TERNLandscapes/Public/Pages/COGs/. The R scripts used to develop the maps and figures for the

https://doi.org/10.5194/bg-2022-207
Preprint. Discussion started: 28 October 2022

paper are publicly available at https://github.com/AusSoilsDSM/SLGA/tree/main/Production/DSM. The spectral models and SOC fraction predictions are available upon reasonable request. The maps can be downloaded from https://data.tern.org.au/landscapes/slga/NationalMaps.

References

Australian Bureau of Agricultural and Resource Economics and Sciences (ABARES). Land use: https://www.agriculture.gov.au/abares/aclump/land-use, last access: 20/09/2022.
Aitchison, J.: Monographs on statistics and applied probability, 1986.
Arrouays, D., McBratney, A. B., Minasny, B., Hempel, J. W., Heuvelink, G., MacMillan, R., Hartemink, A., Lagacherie, P., and McKenzie, N. J.: The GlobalSoilMap project specifications, GlobalSoilMap, 494, 9-12, 2014.
Averill, C., Turner, B. L., and Finzi, A. C.: Mycorrhiza-mediated competition between plants and decomposers drives soil carbon storage, Nature, 505, 543-545, 2014.
Baisden, W. T., Amundson, R., Cook, A. C., and Brenner, D. L.: Turnover and storage of C and N in five density fractions from California annual grassland surface soils, Global Biogeochemical Cycles, 16, 64-61-64-16, https://doi.org/10.1029/2001GB001822, 2002.
Baldock, J., Beare, M., Curtin, D., and Hawke, B.: Stocks, composition and vulnerability to loss of soil organic carbon predicted using mid-infrared spectroscopy, Soil Research, 56, 468-480, 2018.
Baldock, J., Sanderman, J., Macdonald, L., Allen, D., Cowie, A., Dalal, R., Davy, M., Doyle, R., Herrmann, T., Murphy, D., and Robertson, F.: Australian Soil Carbon Research Program. v2. CSIRO. Data Collection [dataset], https://doi.org/10.25919/5ddfd6888d4e5, 2013a.
Baldock, J. A., Hawke, B., Sanderman, J., and Macdonald, L. M.: Predicting contents of carbon and its component fractions in Australian soils from diffuse reflectance mid-infrared spectra, Soil Research, 51, 577-583, 10.1071/Sr13077, 2013b.
Baldock, J. A., Sanderman, J., Macdonald, L. M., Puccini, A., Hawke, B., Szarvas, S., and McGowan, J.: Quantifying the allocation of soil organic carbon to biologically significant fractions, Soil Research, 51, 561-576, 10.1071/Sr12374, 2013c.
Beaudette, D. E., Roudier, P., and Brown, A.: aqp: Algorithms for Quantitative Pedology. R package version 1.42 [code], 2022.
Bennett, L. T., Hinko-Najera, N., Aponte, C., Nitschke, C. R., Fairman, T. A., Fedrigo, M., and Kasel, S.: Refining benchmarks for soil organic carbon in Australia's temperate forests, Geoderma, 368, ARTN 114246 10.1016/j.geoderma.2020.114246, 2020.
Bishop, T. F. A., McBratney, A. B., and Laslett, G. M.: Modelling soil attribute depth functions with equal-area quadratic smoothing splines, Geoderma, 91, 27-45, Doi 10.1016/S0016-7061(99)00003-8, 1999.
Bouveresse, E. and Massart, D. L.: Improvement of the piecewise direct standardisation procedure for the transfer of NIR spectra for multivariate calibration, Chemometrics and Intelligent Laboratory Systems, 32, 201-213, https://doi.org/10.1016/0169-7439(95)00074-7, 1996.
Breiman, L.: Random forests, Mach Learn, 45, 5-32, Doi 10.1023/A:1010933404324, 2001.
Brus, D. J., Kempen, B., and Heuvelink, G. B. M.: Sampling for validation of digital soil maps, Eur J Soil Sci, 62, 394-407, https://doi.org/10.1111/j.1365-2389.2011.01364.x, 2011.
Bui, E., Henderson, B., and Viergever, K.: Using knowledge discovery with data mining from the Australian Soil Resource Information System database to inform soil carbon mapping in Australia, Global Biogeochemical Cycles, 23, https://doi.org/10.1029/2009GB003506, 2009.
Bui, E. N. and Henderson, B. L.: C:N:P stoichiometry in Australian soils with respect to vegetation and environmental factors, Plant Soil, 373, 553-568, 10.1007/s11104-013-1823-9, 2013.
Bunemann, E. K., Bongiorno, G., Bai, Z. G., Creamer, R. E., De Deyn, G., de Goede, R., Fleskens, L., Geissen, V., Kuyper, T. W., Mader, P., Pulleman, M., Sukkel, W., van Groenigen, J. W., and Brussaard, L.: Soil quality - A critical review, Soil Biol Biochem, 120, 105-125, 10.1016/j.soilbio.2018.01.030, 2018.

https://doi.org/10.5194/bg-2022-207
Preprint. Discussion started: 28 October 2022

Conant, R. T., Steinweg, J. M., Haddix, M. L., Paul, E. A., Plante, A. F., and Six, J.: Experimental warming shows that decomposition temperature sensitivity increases with soil organic matter recalcitrance, Ecology, 89, 2384-2391, https://doi.org/10.1890/08-0137.1, 2008.
Congalton, R. G.: A review of assessing the accuracy of classifications of remotely sensed data, Remote Sensing of Environment, 37, 35-46, https://doi.org/10.1016/0034-4257(91)90048-B, 1991.
Cotrufo, M. F., Ranalli, M. G., Haddix, M. L., Six, J., and Lugato, E.: Soil carbon storage informed by particulate and mineral-associated organic matter, Nat Geosci, 12, 989-+, 10.1038/s41561-019-0484-6, 2019.
Cotrufo, M. F., Soong, J. L., Horton, A. J., Campbell, E. E., Haddix, Michelle L., Wall, D. H., and Parton, W. J.: Formation of soil organic matter via biochemical and physical pathways of litter mass loss, Nat Geosci, 8, 776-779, 10.1038/ngeo2520, 2015.
Doetterl, S., Cornelis, J. T., Six, J., Bodé, S., Opfergelt, S., Boeckx, P., and Van Oost, K.: Soil redistribution and weathering controlling the fate of geochemical and physical carbon stabilization mechanisms in soils of an eroding landscape, Biogeosciences, 12, 1357-1371, 10.5194/bg-12-1357-2015, 2015a.
Doetterl, S., Stevens, A., Six, J., Merckx, R., Van Oost, K., Pinto, M. C., Casanova-Katny, A., Munoz, C., Boudin, M., Venegas, E. Z., and Boeckx, P.: Soil carbon storage controlled by interactions between geochemistry and climate, Nat Geosci, 8, 780-+, 10.1038/Ngeo2516, 2015b.
Donohue, R., McVicar, T., and Roderick, M.: Fraction of Photosynthetically Active Radiation (FPAR) - AVHRR (5), Terrestrial Ecosystem Research Network [dataset], 2021.
Dutta, R., Das, A., and Aryal, J.: Big data integration shows Australian bush-fire frequency is increasing significantly, Roy Soc Open Sci, 3, ARTN 150241
10.1098/rsos.150241, 2016.
Farr, T. G., Rosen, P. A., Caro, E., Crippen, R., Duren, R., Hensley, S., Kobrick, M., Paller, M., Rodriguez, E., and Roth, L.: The shuttle radar topography mission, Reviews of geophysics, 45, 2007.
Friedlingstein, P., O'Sullivan, M., Jones, M. W., Andrew, R. M., Hauck, J., Olsen, A., Peters, G. P., Peters, W., Pongratz, J., Sitch, S., Le Quere, C., Canadell, J. G., Ciais, P., Jackson, R. B., Alin, S., Aragao, L. E. O. C., Arneth, A., Arora, V., Bates, N. R., Becker, M., Benoit-Cattin, A., Bittig, H. C., Bopp, L., Bultan, S., Chandra, N., Chevallier, F., Chini, L. P., Evans, W., Florentie, L., Forster, P. M., Gasser, T., Gehlen, M., Gilfillan, D., Gkritzalis, T., Gregor, L., Gruber, N., Harris, I., Hartung, K., Haverd, V., Houghton, R. A., Ilyina, T., Jain, A. K., Joetzjer, E., Kadono, K., Kato, E., Kitidis, V., Korsbakken, J. I., Landschutzer, P., Lefevre, N., Lenton, A., Lienert, S., Liu, Z., Lombardozzi, D., Marland, G., Metzl, N., Munro, D. R., Nabel, J. E. M. S., Nakaoka, S. I., Niwa, Y., O'Brien, K., Ono, T., Palmer, P. I., Pierrot, D., Poulter, B., Resplandy, L., Robertson, E., Rodenbeck, C., Schwinger, J., Seferian, R., Skjelvan, I., Smith, A. J. P., Sutton, A. J., Tanhua, T., Tans, P. P., Tian, H., Tilbrook, B., Van der Werf, G., Vuichard, N., Walker, A. P., Wanninkhof, R., Watson, A. J., Willis, D., Wiltshire, A. J., Yuan, W. P., Yue, X., and Zaehle, S.: Global Carbon Budget 2020, Earth Syst Sci Data, 12, 3269-3340, 10.5194/essd-12-3269-2020, 2020.
Gallant, J. C. and Austin, J. M.: Derivation of terrain covariates for digital soil mapping in Australia, Soil Research, 53, 895-906, https://doi.org/10.1071/SR14271, 2015.
Gallant, J. C. and Dowling, T. I.: A multiresolution index of valley bottom flatness for mapping depositional areas, Water Resour Res, 39, 10.1029/2002WR001426, 2003.
Ge, Y., Morgan, C. L. S., Grunwald, S., Brown, D. J., and Sarkhot, D. V.: Comparison of soil reflectance spectra and calibration models obtained using multiple spectrometers, Geoderma, 161, 202-211, https://doi.org/10.1016/j.geoderma.2010.12.020, 2011.
Geng, J., Cheng, S. L., Fang, H. J., Pei, J., Xu, M., Lu, M. Z., Yang, Y., Cao, Z. C., and Li, Y. N.: Different Molecular Characterization of Soil Particulate Fractions under N Deposition in a Subtropical Forest, Forests, 10, ARTN 914
10.3390/f10100914, 2019.
Gregorich, E. G., Beare, M. H., Mckim, U. F., and Skjemstad, J. O.: Chemical and biological characteristics of physically uncomplexed organic matter, Soil Sci Soc Am J, 70, 975-985, 2006.
Grundy, M. J., Rossel, R. A. V., Searle, R. D., Wilson, P. L., Chen, C., and Gregory, L. J.: Soil and Landscape Grid of Australia, Soil Research, 53, 835-844, https://doi.org/10.1071/SR15191, 2015.
Harper, R. J., Gilkes, R. J., Hill, M. J., and Carter, D. J.: Wind erosion and soil carbon dynamics in south-western Australia, Aeolian Research, 1, 129-141, https://doi.org/10.1016/j.aeolia.2009.10.003, 2010.

https://doi.org/10.5194/bg-2022-207
Preprint. Discussion started: 28 October 2022

Harris, S. and Lucas, C.: Understanding the variability of Australian fire weather between 1973 and 2017, Plos One, 14, e0222328, 10.1371/journal.pone.0222328, 2019.
Hartley, I. P., Hill, T. C., Chadburn, S. E., and Hugelius, G.: Temperature effects on carbon storage are controlled by soil stabilisation capacities, Nat Commun, 12, 6713, 10.1038/s41467-021-27101-1, 2021.
Harwood, T.: 9s climatology for continental Australia 1976-2005: BIOCLIM variable suite. v1. [dataset], https://doi.org/10.25919/5dce30cad79a8, 2019.
Heckman, K., Pries, C. E. H., Lawrence, C. R., Rasmussen, C., Crow, S. E., Hoyt, A. M., von Fromm, S. F., Shi, Z., Stoner, S., McGrath, C., Beem-Miller, J., Berhe, A. A., Blankinship, J. C., Keiluweit, M., Marin-Spiotta, E., Monroe, J. G., Plante, A. F., Schimel, J., Sierra, C. A., Thompson, A., and Wagai, R.: Beyond bulk: Density fractions explain heterogeneity in global soil carbon abundance and persistence, Global Change Biol, 28, 1178-1196, 10.1111/gcb.16023, 2022.
Hicks, W., Rossel, R. V., and Tuomi, S.: Developing the Australian mid-infrared spectroscopic database using data from the Australian Soil Resource Information System, Soil Research, 53, 922-931, 2015.
Hurlbut, C. S. and Klein, C.: Manual of mineralogy (after James D. Dana), Wiley1977.
Iooss, B., Da Veiga, S., Janon, A., and Pujol, G.: sensitivity: Global Sensitivity Analysis of Model Outputs. R package version 1.27.0., 2021.
Isbell, R. F., McDonald, W. S., and Ashton, L. J.: Concepts and rationale of the Australian Soil Classification, CSIRO Land and Water1997.
Jenkinson, D. S. and Rayner, J. H.: The turnover of soil organic matter in some of the Rothamsted classical experiments, Soil science, 123, 298-305, 1977.
Jia, Y., Kuzyakov, Y., Wang, G., Tan, W., Zhu, B., and Feng, X.: Temperature sensitivity of decomposition of soil organic matter fractions increases with their turnover time, Land Degrad Dev, 31, 632-645, https://doi.org/10.1002/ldr.3477, 2020.
Jo, I., Fei, S. L., Oswalt, C. M., Domke, G. M., and Phillips, R. P.: Shifts in dominant tree mycorrhizal associations in response to anthropogenic impacts, Sci Adv, 5, 2019.
Jobbagy, E. G. and Jackson, R. B.: The vertical distribution of soil organic carbon and its relation to climate and vegetation, Ecol Appl, 10, 423-436, Doi 10.2307/2641104, 2000.
Johansen, K., Gill, T., Trevithick, R., Armston, J., Scarth, P., Flood, N., and Phinn, S.: Landsat based Persistent Green-Vegetation Fraction for Australia, Proceedings of the 16th Australasian Remote Sensing and Photogrammery Conference,
Joint Remote Sensing Research, P.: Seasonal fractional cover - Landsat, JRSRP algorithm, Australia coverage (1.0.0), Terrestrial Ecosystem Research Network [dataset], 2021.
Kallenbach, C. M., Frey, S. D., and Grandy, A. S.: Direct evidence for microbial-derived soil organic matter formation and its ecophysiological controls, Nat Commun, 7, 1-10, 2016.
Kleber, M., Sollins, P., and Sutton, R.: A conceptual model of organo-mineral interactions in soils: self-assembly of organic molecular fragments into zonal structures on mineral surfaces, Biogeochemistry, 85, 9-24, 10.1007/s10533-007-9103-5, 2007.
Kleber, M., Eusterhues, K., Keiluweit, M., Mikutta, C., Mikutta, R., and Nico, P. S.: Mineral-Organic Associations: Formation, Properties, and Relevance in Soil Environments, Adv Agron, 130, 1-140, 10.1016/bs.agron.2014.10.005, 2015.
Knicker, H.: Soil organic N - An under-rated player for C sequestration in soils?, Soil Biol Biochem, 43, 1118-1129, 10.1016/j.soilbio.2011.02.020, 2011.
Lane, R. J. L., Wynne, P. E., Poudjom Djomani, Y. H., Stratford, W. R., Barretto, J. A., and Caratori Tontini, F.: 2019 Australian National Gravity Grids [dataset], 2020.
Lavallee, J. M., Soong, J. L., and Cotrufo, M. F.: Conceptualizing soil organic matter into particulate and mineral-associated forms to address global change in the 21st century, Global Change Biol, 26, 261-273, 10.1111/gcb.14859, 2020.
Lavallee, J. M., Conant, R. T., Haddix, M. L., Follett, R. F., Bird, M. I., and Paul, E. A.: Selective preservation of pyrogenic carbon across soil organic matter fractions and its influence on calculations of carbon mean residence times, Geoderma, 354, 113866, https://doi.org/10.1016/j.geoderma.2019.07.024, 2019.
Lehmann, J. and Kleber, M.: The contentious nature of soil organic matter, Nature, 528, 60-68, 10.1038/nature16069, 2015.
Lehmann, J., Skjemstad, J., Sohi, S., Carter, J., Barson, M., Falloon, P., Coleman, K., Woodbury, P., and Krull, E.: Australian climate–carbon cycle feedback reduced by soil black carbon, Nat Geosci, 1, 832-835, 10.1038/ngeo358, 2008.
Li, D., Schädel, C., Haddix, M. L., Paul, E. A., Conant, R., Li, J., Zhou, J., and Luo, Y.: Differential responses of soil organic carbon fractions to warming: Results from an analysis with data assimilation, Soil Biology and Biochemistry, 67, 24-30, https://doi.org/10.1016/j.soilbio.2013.07.008, 2013.

Li, J. Q., Nie, M., Powell, J. R., Bissett, A., and Pendall, E.: Soil physico-chemical properties are critical for predicting carbon storage and nutrient availability across Australia, Environ Res Lett, 15, ARTN 094088 10.1088/1748-9326/ab9f7e, 2020.

Liang, C., Amelung, W., Lehmann, J., and Kästner, M.: Quantitative assessment of microbial necromass contribution to soil organic matter, Global Change Biol, 25, 3578-3590, https://doi.org/10.1111/gcb.14781, 2019.

Lin, L. I.-K.: A concordance correlation coefficient to evaluate reproducibility, Biometrics, 45, 255-268, 10.2307/2532051, 1989.

Lugato, E., Lavallee, J. M., Haddix, M. L., Panagos, P., and Cotrufo, M. F.: Different climate sensitivity of particulate and mineral-associated soil organic matter (vol 14, pg 295, 2021), Nat Geosci, 15, 509-509, 10.1038/s41561-022-00945-y, 2022.

Lutfalla, S., Abiven, S., Barré, P., Wiedemeier, D. B., Christensen, B. T., Houot, S., Kätterer, T., Macdonald, A. J., van Oort, F., and Chenu, C.: Pyrogenic Carbon Lacks Long-Term Persistence in Temperate Arable Soils, Front Earth Sc-Switz, 5, 10.3389/feart.2017.00096, 2017.

Lutzow, M. v., Kogel-Knabner, I., Ekschmitt, K., Flessa, H., Guggenberger, G., Matzner, E., Marschner, B., and von Lutzow, M.: SOM fractionation methods: relevance to functional pools and to stabilization mechanisms, Soil Biol Biochem, 39, 2183-2207, 10.1016/j.soilbio.2007.03.007, 2007.

Lutzow, M. v., Kogel-Knabner, I., Ekschmitt, K., Matzner, E., Guggenberger, G., Marschner, B., Flessa, H., and v. Lutzow, M.: Stabilization of organic matter in temperate soils: mechanisms and their relevance under different soil conditions - a review, Eur J Soil Sci, 57, 426-445, 10.1111/j.1365-2389.2006.00809.x, 2006.

Lymburner, L., Tan, P., Mueller, N., Thackway, R., Thankappan, M., Islam, A., Lewis, A., Randall, L., and Senarath, U.: The National Dynamic Land Cover Dataset [dataset], 2010.

Malley, J. D., Kruppa, J., Dasgupta, A., Malley, K. G., and Ziegler, A.: Probability machines, Methods of information in medicine, 51, 74-81, 2012.

Malone, B.: Soil carbon fraction modelling via vis-NIR spectroscopy, CSIRO, Australia, 2021.

Malone, B. and Searle, R.: Improvements to the Australian national soil thickness map using an integrated data mining approach, Geoderma, 377, ARTN 114579 10.1016/j.geoderma.2020.114579, 2020.

Malone, B. and Searle, R.: Updating the Australian digital soil texture mapping (Part 2*): spatial modelling of merged field and lab measurements, Soil Research, 59, 435-451, 10.1071/Sr20284, 2021.

Malone, B. and Wadoux, A. M. J.-C.: Soil carbon fraction model development and extension: A case of instrument transfer and assessment of model extensibility, CSIRO, 2021.

Malone, B., Stockmann, U., Tuomi, S., and Sparrow, B.: TERN Surveillance monitoring program: Soil vis-NIR spectral library with accompanying soil measurement data for 367 specimens. v1. [dataset], https://doi.org/10.25919/9bya-9545, 2020.

Martin, M. P., Dimassi, B., Dobarco, M. R., Guenet, B., Arrouays, D., Angers, D. A., Blache, F., Huard, F., Soussana, J. F., and Pellerin, S.: Feasibility of the 4 per 1000 aspirational target for soil carbon: A case study for France, Global Change Biol, 27, 2458-2477, 10.1111/gcb.15547, 2021.

Martinez, J.-M.: Analyse de sensibilite globale par decomposition de la variance, GdR Ondes and GdR MASCOT-NUM, Institut Henri Poincare,Paris, France, January, 13th, 20112011.

Masek, J. G., Vermote, E. F., Saleous, N. E., Wolfe, R., Hall, F. G., Huemmrich, K. F., Gao, F., Kutler, J., and Lim, T.-K.: A Landsat surface reflectance dataset for North America, 1990-2000, IEEE Geoscience and Remote Sensing Letters, 3, 68-72, 2006.

McBratney, A. B., Santos, M. L. M., and Minasny, B.: On digital soil mapping, Geoderma, 117, 3-52, 10.1016/S0016-7061(03)00223-4, 2003.

McKenzie, N., Coughlan, K., and Cresswell, H.: Soil physical measurement and interpretation for land evaluation, CSIRO publishing2002.

McKenzie, N., Jacquier, D., Isbell, R., and Brown, K.: Australian soils and landscapes: an illustrated compendium, CSIRO publishing2004.

Meinshausen, N.: Quantile regression forests, Journal of Machine Learning Research, 7, 983-999, 2006.

Meyer, N., Bornemann, L., Welp, G., Schiedung, H., Herbst, M., and Amelung, W.: Carbon saturation drives spatial patterns of soil organic matter losses under long-term bare fallow, Geoderma, 306, 89-98, 10.1016/j.geoderma.2017.07.004, 2017.

Miltner, A., Bombach, P., Schmidt-Brucken, B., and Kastner, M.: SOM genesis: microbial biomass as a significant source, Biogeochemistry, 111, 41-55, 10.1007/s10533-011-9658-z, 2012.

Ng, W., Minasny, B., Jeon, S. H., and McBratney, A.: Mid-infrared spectroscopy for accurate measurement of an extensive set of soil properties for assessing soil functions, Soil Security, 6, 100043, https://doi.org/10.1016/j.soisec.2022.100043, 2022.

Olson, D. M., Dinerstein, E., Wikramanayake, E. D., Burgess, N. D., Powell, G. V. N., Underwood, E. C., D'amico, J. A., Itoua, I., Strand, H. E., Morrison, J. C., Loucks, C. J., Allnutt, T. F., Ricketts, T. H., Kura, Y., Lamoreux, J. F., Wettengel, W. W., Hedao, P., and Kassem, K. R.: Terrestrial Ecoregions of the World: A New Map of Life on Earth: A new global map of terrestrial ecoregions provides an innovative tool for conserving biodiversity, BioScience, 51, 933-938, 10.1641/0006-3568(2001)051[0933:Teotwa]2.0.Co;2, 2001.

Poeplau, C., Vos, C., and Don, A.: Soil organic carbon stocks are systematically overestimated by misuse of the parameters bulk density and rock fragment content, Soil, 3, 61-66, 2017.

Poeplau, C., Don, A., Dondini, M., Leifeld, J., Nemo, R., Schumacher, J., Senapati, N., and Wiesmeier, M.: Reproducibility of a soil organic carbon fractionation method to derive RothC carbon pools, Eur J Soil Sci, 64, 735-746, 10.1111/ejss.12088, 2013.

Poeplau, C., Don, A., Six, J., Kaiser, M., Benbi, D., Chenu, C., Cotrufo, M. F., Derrien, D., Gioacchini, P., Grand, S., Gregorich, E., Griepentrog, M., Gunina, A., Haddix, M., Kuzyakov, Y., Kuhnel, A., Macdonald, L. M., Soong, J., Trigalet, S., Vermeire, M. L., Rovira, P., van Wesemael, B., Wiesmeier, M., Yeasmin, S., Yevdokimov, I., and Nieder, R.: Isolating organic carbon fractions with varying turnover rates in temperate agricultural soils - A comprehensive method comparison, Soil Biol Biochem, 125, 10-26, 10.1016/j.soilbio.2018.06.025, 2018.

Rabbi, S. M. F., Linser, R., Hook, J. M., Wilson, B. R., Lockwood, P. V., Daniel, H., and Young, I. M.: Characterization of soil organic matter in aggregates and size-density fractions by solid state 13C CPMAS NMR spectroscopy, Communications in Soil Science and Plant Analysis, 45, 1523-1537, 10.1080/00103624.2014.904335, 2014.

Rasmussen, C., Heckman, K., Wieder, W. R., Keiluweit, M., Lawrence, C. R., Berhe, A. A., Blankinship, J. C., Crow, S. E., Druhan, J. L., Pries, C. E. H., Marin-Spiotta, E., Plante, A. F., Schadel, C., Schimel, J. P., Sierra, C. A., Thompson, A., and Wagai, R.: Beyond clay: towards an improved set of variables for predicting soil organic matter content, Biogeochemistry, 137, 297-306, 10.1007/s10533-018-0424-3, 2018.

Rayment, G. E. and Lyons, D. J.: Soil chemical methods: Australasia, CSIRO publishing2011.

Reisser, M., Purves, R. S., Schmidt, M. W. I., and Abiven, S.: Pyrogenic Carbon in Soils: A Literature-Based Inventory and a Global Estimation of Its Content in Soil Organic Carbon and STocks, Front Earth Sc-Switz, 4, ARTN 80 10.3389/feart.2016.00080, 2016.

Robertson, A. D., Paustian, K., Ogle, S., Wallenstein, M. D., Lugato, E., and Cotrufo, M. F.: Unifying soil organic matter formation and persistence frameworks: the MEMS model, Biogeosciences, 16, 1225-1248, 10.5194/bg-16-1225-2019, 2019.

Rocci, K. S., Lavallee, J. M., Stewart, C. E., and Cotrufo, M. F.: Soil organic carbon response to global environmental change depends on its distribution between mineral-associated and particulate organic matter: A meta-analysis, Sci Total Environ, 793, 148569, https://doi.org/10.1016/j.scitotenv.2021.148569, 2021.

Rowley, M. C., Grand, S., and Verrecchia, E. P.: Calcium-mediated stabilisation of soil organic carbon, Biogeochemistry, 137, 27-49, 10.1007/s10533-017-0410-1, 2018.

Saltelli, A., Ratto, M., Andres, T., Campolongo, F., Cariboni, J., Gatelli, D., Saisana, M., and S., T.: Variance-based methods, in: Global Sensitivity Analysis. The Primer, John Wiley & Sons, Ltd, 2008.

Sanderman, J., Baldock, J., Hawke, B., Macdonald, L., Puccini, A., and Szarvas, S.: National soil carbon research programme: field and laboratory methodologies, 2011.

Sanderman, J., Baldock, J. A., Dangal, S. R. S., Ludwig, S., Potter, S., Rivard, C., and Savage, K.: Soil organic carbon fractions in the Great Plains of the United States: an application of mid-infrared spectroscopy, Biogeochemistry, 156, 97-114, 10.1007/s10533-021-00755-1, 2021.

Sandri, M. and Zuccolotto, P.: A bias correction algorithm for the Gini variable importance measure in classification trees, Journal of Computational and Graphical Statistics, 17, 611-628, 2008.

Scharlemann, J. P. W., Tanner, E. V. J., Hiederer, R., and Kapos, V.: Global soil carbon: understanding and managing the largest terrestrial carbon pool, Carbon Manag, 5, 81-91, 10.4155/Cmt.13.77, 2014.

Schmidt, M. W. I., Torn, M. S., Abiven, S., Dittmar, T., Guggenberger, G., Janssens, I. A., Kleber, M., Kogel-Knabner, I., Lehmann, J., Manning, D. A. C., Nannipieri, P., Rasse, D. P., Weiner, S., and Trumbore, S. E.: Persistence of soil organic matter as an ecosystem property, Nature, 478, 49-56, 10.1038/nature10386, 2011.

Schoenholtz, S. H., Van Miegroet, H., and Burger, J. A.: A review of chemical and physical properties as indicators of forest soil quality: challenges and opportunities, Forest Ecology and Management, 138, 335-356, Doi 10.1016/S0378-1127(00)00423-0, 2000.

Searle, R.: Australian Soil Classification Map [dataset], 10.25901/edyr-wg85, 2021.

Searle, R., Stenson, M., Wilson, P. L., Gregory, L. J., Singh, R., and Malone, B. P.: Soil data, united, will never be defeated – The SoilDataFederator, Joint Australian and New Zealand Soil Science Societies Conference, Cairns, QLD2021.

Shrestha, D. L. and Solomatine, D. P.: Machine learning approaches for estimation of prediction interval for the model output, Neural Networks, 19, 225-235, https://doi.org/10.1016/j.neunet.2006.01.012, 2006.

Singh, N., Abiven, S., Torn, M. S., and Schmidt, M. W. I.: Fire-derived organic carbon in soil turns over on a centennial scale, Biogeosciences, 9, 2847-2857, 10.5194/bg-9-2847-2012, 2012.

Sokol, N. W., Whalen, E. D., Jilling, A., Kallenbach, C., Pett-Ridge, J., and Georgiou, K.: Global distribution, formation and fate of mineral-associated soil organic matter under a changing climate: A trait-based perspective, Funct Ecol, 36, 1411-1429, https://doi.org/10.1111/1365-2435.14040, 2022.

Sollins, P., Homann, P., and Caldwell, B. A.: Stabilization and destabilization of soil organic matter: Mechanisms and controls, Geoderma, 74, 65-105, Doi 10.1016/S0016-7061(96)00036-5, 1996.

Sparrow, B. D., Foulkes, J. N., Wardle, G. M., Leitch, E. J., Caddy-Retalic, S., van Leeuwen, S. J., Tokmakoff, A., Thurgate, N. Y., Guerin, G. R., and Lowe, A. J.: A Vegetation and Soil Survey Method for Surveillance Monitoring of Rangeland Environments, Frontiers in Ecology and Evolution, 8, 10.3389/fevo.2020.00157, 2020.

Terrain, N. C. o. S. a.: Australian soil and land survey field handbook, Third Edition, Australian Soil and Land Survey Handbooks Series 1, 1, CSIRO PUBLISHING, Melbourne, Australia2009.

van den Boogaart, K. G., Tolosana-Delgado, R., and Bren, M.: compositions: Compositional Data Analysis. R package version 2.0-4., 2022.

van Leeuwen, J. P., Creamer, R. E., Cluzeau, D., Debeljak, M., Gatti, F., Henriksen, C. B., Kuzmanovski, V., Menta, C., Peres, G., Picaud, C., Saby, N. P. A., Trajanov, A., Trinsoutrot-Gattin, I., Visioli, G., and Rutgers, M.: Modeling of Soil Functions for Assessing Soil Quality: Soil Biodiversity and Habitat Provisioning, Frontiers in Environmental Science, 7, ARTN 113 10.3389/fenvs.2019.00113, 2019.

Vaysse, K. and Lagacherie, P.: Using quantile regression forest to estimate uncertainty of digital soil mapping products, Geoderma, 291, 55-64, 2017.

Villarino, S. H., Pinto, P., Jackson, R. B., and Piñeiro, G.: Plant rhizodeposition: A key factor for soil organic matter formation in stable fractions, Sci Adv, 7, eabd3176, doi:10.1126/sciadv.abd3176, 2021.

Viscarra Rossel, R. and Hicks, W.: Soil organic carbon and its fractions estimated by visible–near infrared transfer functions, Eur J Soil Sci, 66, 438-450, 2015.

Viscarra Rossel, R. A., Webster, R., Bui, E. N., and Baldock, J. A.: Baseline map of organic carbon in Australian soil to support national carbon accounting and monitoring under climate change, Global Change Biol, 20, 2953-2970, 10.1111/gcb.12569, 2014.

Viscarra Rossel, R. A., Chen, C., Grundy, M. J., Searle, R., Clifford, D., and Campbell, P. H.: The Australian three-dimensional soil grid: Australia's contribution to the GlobalSoilMap project, Soil Research, 53, 845-864, https://doi.org/10.1071/SR14366, 2015.

Viscarra Rossel, R. A., Lee, J., Behrens, T., Luo, Z., Baldock, J., and Richards, A.: Continental-scale soil carbon composition and vulnerability modulated by regional environmental controls, Nat Geosci, 12, 547-+, 10.1038/s41561-019-0373-z, 2019.

von Lutzow, M., Kogel-Knabner, I., Ekschmitt, K., Matzner, E., Guggenberger, G., Marschner, B., and Flessa, H.: Stabilization of organic matter in temperate soils: mechanisms and their relevance under different soil conditions - a review, Eur J Soil Sci, 57, 426-445, 10.1111/j.1365-2389.2006.00809.x, 2006.

von Lützow, M. and Kögel-Knabner, I.: Temperature sensitivity of soil organic matter decomposition—what do we know?, Biol Fert Soils, 46, 1-15, 10.1007/s00374-009-0413-8, 2009.

von Lützow, M., Kögel-Knabner, I., Ekschmitt, K., Flessa, H., Guggenberger, G., Matzner, E., and Marschner, B.: SOM fractionation methods: Relevance to functional pools and to stabilization mechanisms, Soil Biology and Biochemistry, 39, 2183-2207, https://doi.org/10.1016/j.soilbio.2007.03.007, 2007.

Wadoux, A. M. J.-C., Román Dobarco, M., Malone, B., Minasny, M., McBratney, A. B., and Searle, R.: Baseline high-resolution maps of organic carbon content in Australian soils. [dataset], 2022.

Webb, N. P., Chappell, A., Strong, C. L., Marx, S. K., and McTainsh, G. H.: The significance of carbon-enriched dust for global carbon accounting, Global Change Biol, 18, 3275-3278, https://doi.org/10.1111/j.1365-2486.2012.02780.x, 2012.

Wiesmeier, M., Poeplau, C., Sierra, C. A., Maier, H., Frühauf, C., Hübner, R., Kühnel, A., Spörlein, P., Geuß, U., Hangen, E., Schilling, B., von Lützow, M., and Kögel-Knabner, I.: Projected loss of soil organic carbon in temperate agricultural soils in the 21st century: effects of climate change and carbon input trends, Sci Rep-Uk, 6, 32525, 10.1038/srep32525, 2016.

Wiesmeier, M., Urbanski, L., Hobley, E., Lang, B., von Lutzow, M., Marin-Spiotta, E., van Wesemael, B., Rabot, E., Liess, M., Garcia-Franco, N., Wollschlager, U., Vogel, H. J., and Kogel-Knabner, I.: Soil organic carbon storage as a key function of soils - A review of drivers and indicators at various scales, Geoderma, 333, 149-162, 10.1016/j.geoderma.2018.07.026, 2019.

Wilford, J.: A weathering intensity index for the Australian continent using airborne gamma-ray spectrometry and digital terrain analysis, Geoderma, 183, 124-142, 10.1016/j.geoderma.2010.12.022, 2012a.

Wilford, J.: A weathering intensity index for the Australian continent using airborne gamma-ray spectrometry and digital terrain analysis, Geoderma, 183-184, 124-142, https://doi.org/10.1016/j.geoderma.2010.12.022, 2012b.

Wilford, J. and Minty, B.: The use of airborne gamma-ray imagery for mapping soils and understanding landscape processes. In 'Digital soil mapping: an introductory perspective'.(Eds P Lagacherie, AB McBratney, M Voltz) pp. 207–218, 2007.

Wilford, J. R. and Kroll, A.: Complete Radiometric Grid of Australia (Radmap) v4 2019 with modelled infill [dataset], 2020.

Wilson, J. P. and Gallant, J. C.: Secondary topographic attributes, Terrain analysis: Principles and applications, 87-131, 2000.

Wright, M. N. and Ziegler, A.: ranger: A Fast Implementation of Random Forests for High Dimensional Data in C++ and R, Journal of Statistical Software, 77, 1-17, 10.18637/jss.v077.i01, 2017.

Xu, X., Liu, W., and Kiely, G.: Modeling the change in soil organic carbon of grassland in response to climate change: Effects of measured versus modelled carbon pools for initializing the Rothamsted Carbon model, Agriculture, Ecosystems & Environment, 140, 372-381, https://doi.org/10.1016/j.agee.2010.12.018, 2011.

Zevenbergen, L. W. and Thorne, C. R.: Quantitative analysis of land surface topography, Earth Surf Proc Land, 12, 47-56, 1987.

Zhao, P., Li, L., Lin, L., Zhai, G., Cruse, R. M., and Wang, E.: Response of surface soil nutrients and organic carbon fractions to tillage erosion vs. water erosion in an agricultural landscape, Soil Sci Soc Am J, 00, 1– 13, https://doi.org/10.1002/saj2.20461, 2022.

Zimmerman, A. R. and Mitra, S.: Trial by Fire: On the Terminology and Methods Used in Pyrogenic Organic Carbon Research, Front Earth Sc-Switz, 5, 10.3389/feart.2017.00095, 2017.

Zimmermann, M., Leifeld, J., Schmidt, M. W. I., Smith, P., and Fuhrer, J.: Measured soil organic matter fractions can be related to pools in the RothC model, Eur J Soil Sci, 58, 658-667, 10.1111/j.1365-2389.2006.00855.x, 2007.

https://doi.org/10.5194/bg-2022-207
Preprint. Discussion started: 28 October 2022

Biogeosciences Discussions Open Access EGU

Table 2: List of environmental covariates with unit and associated reference when applicable. All covariates are in geographic coordinates with 3 arc second grid cell (about 90 m x 90 m) resolution with coordinate system WGS84 (EPSG:4326) and extent: 112.99958°E - 153.99958°E; 10.0004°S - 44.00042°S.

Factor	Covariate	Predictor variable	Unit	Reference
Soil	Clay	Depth-specific soil clay content (0-5 cm, 5-15 cm, 15-30 cm)	percent	Malone and Searle (2021)
	Sand	Depth-specific soil sand content (0-5 cm, 5-15 cm, 15-30 cm)	percent	Malone and Searle (2021)
Climate	ADM	Mean annual aridity index (annual precipitation/annual potential evaporation)	index	Harwood (2019)
	EPA	Annual potential evaporation	mm	Harwood (2019)
	EPI	Minimum monthly potential evaporation	mm	Harwood (2019)
	EPX	Maximum monthly potential evaporation	mm	Harwood (2019)
	Prescott	Prescott Index generated by using Prescott index = 0.445P / E0.75	index	-
	PTA	Annual precipitation	mm	Harwood (2019)
	PTI	Minimum monthly precipitation	mm	Harwood (2019)
	PTS1	Precipitation seasonality 1- solstice seasonality composite factor ratio	ratio	Harwood (2019)
	PTS2	Precipitation seasonality 2- equinox seasonality composite factor ratio	ratio	Harwood (2019)
	PTX	Maximum monthly precipitation	mm	Harwood (2019)
	RSM	Short-wave solar radiation - annual mean (SRAD data)	MJ/m2/day	Harwood (2019)
	TNM	Minimum temperature – Annual mean	°C	Harwood (2019))
	TRA	Annual temperature range	°C	Harwood (2019
	TXM	Maximum temperature - Annual mean	°C	Harwood (2019)
	WDA	Annual atmospheric water deficit (annual precipitation – annual potential evaporation)	mm	Harwood (2019)
Organisms/ Vegetation	NDVI_Q1	Landsat 5 long-term average NDVI (January-March) 1986-2011	unitless	U.S. Geological Survey Landsat 5 Surface Reflectance Tier 1. Masek et al. (2006)
	NDVI_Q2	Landsat 5 long-term average NDVI (April-June) 1986- 2011	unitless	U.S. Geological Survey Landsat 5 Surface Reflectance Tier 1. Masek et al. (2006)

https://doi.org/10.5194/bg-2022-207
Preprint. Discussion started: 28 October 2022

NDVI_Q3	Landsat 5 long-term average NDVI (July-September) 1986-2011	unitless	U.S. Geological Survey Landsat 5 Surface Reflectance Tier 1. Masek et al. (2006)
NDVI_Q4	Landsat 5 long-term average NDVI (October-December) 1986 - 2011	unitless	U.S. Geological Survey Landsat 5 Surface Reflectance Tier 1. Masek et al. (2006)
FC_Max_BS	Landsat Fractional cover - Bare Soil -Maximum (1987 – 2019)	percent	Joint Remote Sensing Research Program (2021)
FC_Max_NPV	Landsat Fractional cover - Non Photosynthetic Vegetation - Maximum (1987 – 2019)	percent	Joint Remote Sensing Research Program (2021)
FC_Max_PV	Landsat Fractional cover - Photosynthetic Vegetation - Maximum (1987 – 2019)	percent	Joint Remote Sensing Research Program (2021)
FC_Mean_BS	Landsat Fractional cover - Bare Soil - Mean (1987 – 2019)	percent	Joint Remote Sensing Research Program (2021)
FC_Mean_NPV	Landsat Fractional cover - Non Photosynthetic Vegetation - Mean (1987 – 2019)	percent	Joint Remote Sensing Research Program (2021)
FC_Mean_PV	Landsat Fractional cover - Photosynthetic Vegetation - Mean (1987 – 2019)	percent	Joint Remote Sensing Research Program (2021)
FC_Min_BS	Landsat Fractional cover - Bare Soil Minimum (1987 – 2019)	percent	Joint Remote Sensing Research Program (2021)
FC_Min_NPV	Landsat Fractional cover - Non Photosynthetic Vegetation - Minimum (1987 – 2019)	percent	Joint Remote Sensing Research Program (2021)
FC_Min_PV	Landsat Fractional cover - Photosynthetic Vegetation - Minimum (1987 – 2019)	percent	Joint Remote Sensing Research Program (2021)
FC_SD_BS	Landsat Fractional cover - Bare Soil - Standard deviation (1987 – 2019)	percent	Joint Remote Sensing Research Program (2021)
FC_SD_NPV	Landsat Fractional cover - Non Photosynthetic Vegetation - Standard deviation (1987 – 2019)	percent	Joint Remote Sensing Research Program (2021)
FC_SD_PV	Landsat Fractional cover - Bare Soil - Standard deviation (1987 – 2019)	percent	Joint Remote Sensing Research (2021)
FPAR_Max	Fraction of Photosynthetically Active Radiation (FPAR) - AVHRR - Maximum Value in time series	percent	Donohue et al. (2021)
FPAR_Mean	Fraction of Photosynthetically Active Radiation (FPAR) - AVHRR - Mean Value in time series	percent	Donohue et al. (2021)
FPAR_Median	Fraction of Photosynthetically Active Radiation (FPAR) - AVHRR - Median Value in time series	percent	Donohue et al. (2021)

https://doi.org/10.5194/bg-2022-207
Preprint. Discussion started: 28 October 2022

	FPAR_Min	Fraction of Photosynthetically Active Radiation (FPAR) - AVHRR - Minimum Value in time series	percent	Donohue et al. (2021)
	LC_EVI	National Dynamic Land Cover Dataset Mean of enhanced vegetation index (EVI) for the timeseries 2000 – 2008	unitless	Lymburner et al. (2010)
	Pers_Green_Veg	Landsat 2000-2010 Persistent Green-Vegetation Fraction	unitless	Johansen et al. (2012)
Relief	DEM	Elevation 3 Second - Shuttle Radar Topography Mission	meter	Farr et al. (2007)
	MRRTF	Multi-resolution Ridgetop Flatness	unitless	Gallant and Austin (2015)
	MRVBF	Multiresolution Index of Valley Bottom Flatness	unitless	Gallant and Dowling (2003)
	Plan_curv	Plan curvature	unitless	Wilson and Gallant (2000)
	Prof_curv	Profile curvature	unitless	Wilson and Gallant (2000)
	Roughness	Relief roughness	unitless	Wilson and Gallant (2000)
	Slope	Slope	percent	Zevenbergen and Thorne (1987)
	TWI	Topographic wetness index	unitless	Wilson and Gallant (2000)
Parent material/ Age	Gravity	Gravity Anomaly Grid of Australia	unitless	Lane et al. (2020)
	Dose	Radiometric grid of Australia (Radmap) v4 2019 - Filtered dose	unitless	Wilford and Kroll (2020)
	K	Radiometric grid of Australia (Radmap) v4 2019 - Potassium	percent	Wilford and Kroll (2020)
	Th	Radiometric grid of Australia (Radmap) v4 2019 - Thorium	ppm	Wilford and Kroll (2020)
	U	Radiometric grid of Australia (Radmap) v4 2019 - Uranium	ppm	Wilford and Kroll (2020)
	Th_K	Radiometric grid of Australia (Radmap) v4 2019 - Thorium Potassium ratio	ratio	Wilford and Kroll (2020)
	U2_Th	Radiometric grid of Australia (Radmap) v4 2019 - Uranium squared to Thorium ratio	ratio	Wilford and Kroll (2020)
	U_K	Radiometric grid of Australia (Radmap) v4 2019 - Uranium Potassium ratio	ratio	Wilford and Kroll (2020)
	U_Th	Radiometric grid of Australia (Radmap) v4 2019 - Uranium Thorium ratio	ratio	Wilford and Kroll (2020)
	WII	Weathering intensity index	unitless	Wilford (2012b)

995